

# An Effective Model of the Retinoic Acid Induced HL-60 Differentiation Program

Ryan Tasseff, Holly A. Jensen, Wei Dai, Katherine Rogers, Adithya Sagar, Rodica P. Bunaciu<sup>†</sup>, Johanna Congleton<sup>†</sup>, Andrew Yen<sup>†</sup>, and Jeffrey D. Varner\*

Robert Frederick Smith School of Chemical and Biomolecular Engineering and <sup>†</sup>Department of Biomedical Sciences, Cornell University, Ithaca NY 14853

**Running Title:** Effective modeling of HL-60 differentiation

**To be submitted:** *Frontiers in Systems Biology*

\*Corresponding author:

Jeffrey D. Varner,

Professor, Robert Frederick Smith School of Chemical and Biomolecular Engineering,  
244 Olin Hall, Cornell University, Ithaca NY, 14853

Email: jdv27@cornell.edu

Phone: (607) 255 - 4258

Fax: (607) 255 - 9166

## **Abstract**

In this study, we present an effective model All-Trans Retinoic Acid (ATRA)-induced differentiation of HL-60 cells. The model describes a key architectural feature of ATRA-induced differentiation, positive feedback between an ATRA-inducible signalsome complex involving many proteins including Vav1, a guanine nucleotide exchange factor, and the activation of the mitogen activated protein kinase (MAPK) cascade. The model, which was developed by integrating logical rules with kinetic modeling, was significantly smaller than previous models. However, despite its simplicity, it captured key features of ATRA induced differentiation of HL-60 cells. We identified an ensemble of effective model parameters using measurements taken from ATRA-induced HL-60 cells. Using these parameters, model analysis predicted that MAPK activation was bistable as a function of ATRA exposure. Conformational experiments supported ATRA-induced bistability. These findings, combined with other literature evidence, suggest that positive feedback is central to a diversity of cell fate programs.

## **1 Introduction**

2 Understanding the architecture of differentiation programs is an important therapeutic  
3 challenge. Differentiation induction chemotherapy (DIC), using agents such as the vita-  
4 min A derivative all-trans retinoic acid (ATRA), is a promising approach for the treatment  
5 of many cancers (1–3). For example, ATRA treatment induces remission in 80–90% of  
6 promyelocytic leukemia (APL) PML-RAR $\alpha$ -positive patients (4), thereby transforming a  
7 fatal diagnosis into a manageable disease. However, remission is sometimes not durable  
8 and relapsed cases exhibit emergent ATRA resistance (5, 6). To understand the basis of  
9 this resistance, we must first understand the ATRA-induced differentiation program. To-  
10 ward this challenge, lessons learned in model systems, such as the lineage-uncommitted  
11 human myeloblastic cell line HL-60, could inform our analysis of the more complex dif-  
12 ferentiation programs occurring in patients. Patient derived HL-60 leukemia cells have  
13 been a durable experimental model since the 1970's to study differentiation (7). HL-60  
14 undergoes cell cycle arrest and either myeloid or monocytic differentiation following stim-  
15 ulation; ATRA induces G1/G0-arrest and myeloid differentiation in HL-60 cells, while 1,25-  
16 dihydroxy vitamin D3 (D3) induces arrest and monocytic differentiation. Commitment to  
17 cell cycle arrest and differentiation requires approximately 48 hr of treatment, during which  
18 HL-60 cells undergo two division cycles.

19 Sustained mitogen-activated protein kinase (MAPK) activation is a defining feature of  
20 ATRA-induced HL-60 differentiation. ATRA drives sustained MEK-dependent activation  
21 of the Raf/MEK/ERK pathway, leading to arrest and differentiation (8). MEK inhibition re-  
22 sults in the loss of ERK and Raf phosphorylation, and the failure to arrest and differentiate  
23 (9). ATRA (and its metabolites) are ligands for the hormone activated nuclear transcrip-  
24 tion factors retinoic acid receptor (RAR) and retinoid X receptor (RXR) (10). RAR/RXR  
25 activation is necessary for ATRA-induced Raf phosphorylation (9), and the formation of  
26 an ATRA-inducible signalsome complex at the membrane which drives MAPK activation

27 through a yet to be identified kinase activity. While the makeup of the signalsome com-  
28 plex is not yet known, we do know that it is composed of Src family kinases Fgr and Lyn,  
29 PI3K, c-Cbl, Slp76, and KSR, as well as IRF-1 transcription factors (11–15). Signalsome  
30 formation and activity is driven by ATRA-induced expression of CD38 and the putative  
31 heterotrimeric Gq protein-coupled receptor BLR1 (16, 17). BLR1, identified as an early  
32 ATRA (or D3)-inducible gene using differential display (18), is necessary for MAPK ac-  
33 tivation and differentiation (17), and is also involved with signalsome activity. Studies  
34 of the BLR1 promoter identified a 5' 17bp GT box approximately 1 kb upstream of the  
35 transcriptional start that conferred ATRA responsiveness (17). Members of the BLR1  
36 transcriptional activator complex, e.g. NFATc3 and CREB, are phosphorylated by ERK,  
37 JNK or p38 MAPK family members suggesting positive feedback between the signalsome  
38 and MAPK activation (19). BLR1 overexpression enhanced Raf phosphorylation and ac-  
39 celerated terminal differentiation, while Raf inhibition reduced BLR1 expression and dif-  
40 ferentiation (20). BLR1 knock-out cells failed to activate Raf or differentiate in the pres-  
41 ence of ATRA (20). Interestingly, both the knockdown or inhibition of Raf, also reduced  
42 BLR1 expression and functional differentiation (20). Thus, the expression of signalsome  
43 components e.g., BLR1 was Raf dependent, while Raf activation depended upon the sig-  
44 nalsome. A recent computational study of ATRA-induced differentiation in HL-60 cells  
45 suggested that the BLR1-MAPK positive feedback circuit was sufficient to explain ATRA-  
46 induced sustained MAPK activation, and the expression of a limited number of functional  
47 differentiation markers (21). Model analysis also suggested that Raf was the most distinct  
48 of the MAPK proteins. However, this previous study developed and analyzed a complex  
49 model, thus leaving open the critical question of what is the minimal positive feedback  
50 circuit required to drive ATRA-induced differentiation.

51 In this study, we explored this question using a minimal mathematical model of the  
52 key architectural feature of ATRA induced differentiation of HL-60 cells, namely positive

53 feedback between an ATRA-inducible signalsome complex and MAPK activation. The  
54 ATRA responsive signalsome-MAPK circuit was then used to drive a downstream gene  
55 expression program which encoded for the expression of functional differentiation mark-  
56 ers. The effective model used a novel framework which integrated logical rules with ki-  
57 netic modeling to describe gene expression and protein regulation, while largely relying  
58 upon biophysical parameters from the literature. This formulation significantly reduced  
59 the size and complexity of the model compared to the previous study of Tasseff et al.,  
60 while increasing the breadth of the biology described (21). The effective model, despite  
61 its simplicity, captured key features of ATRA induced differentiation of HL-60 cells. Model  
62 analysis predicted the bistability of MAPK activation as a function of ATRA exposure; con-  
63 formational experiments supported ATRA-induced bistability. Model simulations were also  
64 consistent with measurements of the influence of MAPK inhibitors, and the failure of BLR1  
65 knockout cells to differentiate when exposed to ATRA. Lastly, we showed by through im-  
66 munoprecipitation studies, that the guanine nucleotide exchange factor Vav1 is potentially  
67 a new ATRA-inducible member of the signalsome complex. Taken together, these findings  
68 when combined with other literature evidence, suggested that positive feedback architec-  
69 tures are central to differentiation programs generally, and necessary for ATRA-induced  
70 differentiation.

71 **Results**

72 We constructed an effective model of ATRA-induced HL-60 differentiation which described  
73 signaling and gene expression events following the addition of ATRA (Fig. 1). The model  
74 connectivity was developed from literature and the studies presented here (Table 1). We  
75 decomposed the ATRA program into three modules; a signal initiation module that sensed  
76 and transformed the ATRA signal into activated cRaf-pS621 and the ATRA-RXR/RAR  
77 (Trigger) signals (Fig. 1A); a signal integration module that controlled the expression of  
78 upstream transcription factors given cRaf-pS621 and activated Trigger signals (Fig. 1B);  
79 and a phenotype module which encoded the expression of functional differentiation mark-  
80 ers from the ATRA-inducible transcription factors (Fig. 1C). Each component of these  
81 modules was described by a mRNA and protein balance equation. Additionally, the sig-  
82 nal initiation module also described the abundance of activated species e.g., Trigger and  
83 cRaf-pS621 whose values were derived from unactivated Trigger and cRaf protein levels.  
84 Lastly, because the population of HL-60 cells was dividing (at least before ATRA-induced  
85 cell cycle arrest), we also considered a dilution term in all balance equations. The sig-  
86 nal initiation module contained nine differential equations, while the signal integration and  
87 phenotype modules were collectively encoded by 54 differential equations. Model param-  
88 eters were taken literature (Table 2), or estimated from experimental data using heuristic  
89 optimization (see materials and methods).

90 The signal initiation module recapitulated sustained signalsome and MAPK activation  
91 following exposure to  $1\mu\text{M}$  ATRA (Fig. 2A-B). An ensemble of effective model param-  
92 eters was estimated by minimizing the difference between simulations and time-series  
93 measurements of BLR1 mRNA and cRaf-pS621 following the addition of  $1\mu\text{M}$  ATRA. We  
94 focused on the S621 phosphorylation site of cRaf since enhanced phosphorylation at  
95 this site is a defining characteristic of sustained MAPK activation in HL-60. The effective  
96 model captured both ATRA-induced BLR1 expression (Fig. 2A) and sustained phospho-

97 phosphorylation of cRaf-pS621 (Fig. 2B) in a growing population of HL-60 cells. Together, the  
98 reinforcing positive feedback between the signalsome and MAPK led to sustained activation  
99 over multiple cellular generations. However, the effective model failed to capture the  
100 decline of BLR1 message after 48 hr of ATRA exposure. This suggested that we captured  
101 the logic leading to the onset of differentiation, but failed to describe program shutdown.  
102 Next, we tested the response of the signal initiation module to different ATRA dosages.

103 The signal initiation model was bistable with respect to ATRA induction (Fig. 2C-D).  
104 Phaseplane analysis predicted two stable steady-states when ATRA was present below  
105 a critical threshold, and only a single steady-state above the threshold (Fig. 2C). In the  
106 lower stable state, neither the signalsome nor cRaf-pS621 were present (thus, the differ-  
107 entiation program was deactivated). However, at the high stable state, both the signal-  
108 some and cRaf-pS621 were present, allowing for sustained activation and differentiation.  
109 Interestingly, when ATRA was above a critical threshold, only the activated state was ac-  
110 cessible (Fig. 2D). To test these findings, we first identified the ATRA threshold. We  
111 exposed HL-60 cells to different ATRA concentrations for 72 hr (Fig. 2E). Morphological  
112 changes associated with differentiation were visible for ATRA  $\geq$  0.25  $\mu$ M, suggesting the  
113 critical ATRA threshold was near this concentration. Next, we conducted ATRA washout  
114 experiments to determine if activated cells remained activated in the absence of ATRA.  
115 HL-60 cells locked into an activated state remained activated following ATRA withdraw-  
116 (Fig. 3). This sustained activation resulted from reinforcing feedback between the sig-  
117 nalsome and the MAPK pathway. Thus, following activation, if we inhibited or removed  
118 elements from the signal initiation module we expected the signalsome and MAPK signals  
119 to decay. We simulated ATRA induced activation in the presence of kinase inhibitors, and  
120 without key circuit elements. Consistent with experimental results using multiple MAPK  
121 inhibitors, ATRA activation in the presence of MAPK inhibitors lowered the steady-state  
122 value of signalsome (Fig. 3A). In the presence of BLR1, the signalsome and cRaf-pS621

123 signals were maintained following ATRA withdraw (Fig. 3B, gray). On the other hand,  
124 BLR1 deletion removed the ability of the circuit to maintain a sustained MAPK response  
125 following the withdraw of ATRA (Fig. 3B, blue). Lastly, washout experiments in which  
126 cells were exposed to  $1\mu\text{M}$  ATRA for 24 hr, and then transferred to fresh media with-  
127 out ATRA, confirmed the persistence of the self sustaining activated state for up to 144  
128 hr (Fig. 3C). Thus, these experiments confirmed that reinforcing positive feedback likely  
129 drives the ATRA-induced differentiation program. Next, we analyzed the ATRA-induced  
130 downstream gene expression program following signalsome and cRaf activation.

131 The signal integration and phenotype modules described ATRA-induced gene expres-  
132 sion in wild-type HL-60 cells (Fig. 4). The signal initiation module produced two outputs,  
133 activated Trigger and cRaf-pS621 which drove the expression of ATRA-induced transcrip-  
134 tion factors, which then in turn activated the phenotypic program. In particular, Trigger,  
135 which is a surrogate for the RAR $\alpha$ /RXR transcriptional complex, regulated the expres-  
136 sion of the transcription factors CCATT/enhancer binding protein  $\alpha$  (C/EBP $\alpha$ ), PU.1, and  
137 EGR1. In turn, these transcription factors, in combination with cRaf-pS621, regulated the  
138 expression of downstream phenotypic markers such as CD38, CD11b or P47Phox. We  
139 assembled the connectivity of the signal integration and phenotypic programs driven by  
140 Trigger and cRaf-pS621 from literature (Table 1). We estimated the parameters which  
141 appeared in the control laws regulating these programs from steady-state and dynamic  
142 measurements of transcription factor and phenotypic marker expression following the ad-  
143 dition of ATRA (22–25). However, the bulk of the remaining model parameters were taken  
144 from directly from literature (26) and were not estimated in this study (see materials and  
145 methods). The model simulations captured the time dependent expression of CD38 and  
146 CD11b following the addition ATRA (Fig. 4A), and the steady-state for signal integration  
147 and phenotypic markers (Fig. 4B). Lastly, we used the *predicted* values of the p21 and  
148 E2F protein abundance to estimate a blackbox model of ATRA-induced G0 arrest (Fig.

149 5). The phenotype module predicted p21 expression significantly increased and E2F ex-  
150 pression decreased, in response to ATRA exposure (Fig. 5A). We then used the ratio of  
151 these values in a polynomial model to calculate the fraction of HL-60 cells in G0 arrest  
152 following the addition of ATRA (Fig. 5B). The third-order polynomial model captured the  
153 trend in measured G0-arrest values as a function of time, and was robust to uncertainty  
154 in the measured data (Fig. 5B, gray). Taken together, the output of the signal integra-  
155 tion and phenotypic modules was consistent with time-series and steady-state measure-  
156 ments, thereby validating the assumed molecular connectivity. Moreover, outputs from  
157 the phenotype module described the trend in ATRA-induced G0 cell cycle arrest. Next,  
158 we explored which nodes and interactions between nodes in the signal integration module  
159 most influenced the system response.

160 The PU.1 and AP1 proteins were important regulators of the ATRA-induced signal in-  
161 tegration and phenotypic programs (Fig. 6). We conducted pairwise knock simulations  
162 of genes in the signal integration and phenotype modules to estimate which nodes con-  
163 trolled the processing of the Trigger and cRaF-S621 signals. The difference between the  
164 system state with and without the gene knockouts (encoded as a state displacement ma-  
165 trix) was decomposed using Singular Value Decomposition (SVD). All simulations were  
166 conducted using the best fit parameter set. The first four modes described >99% of the  
167 gene knockout variance, with the most important components of these modes being the  
168 PU.1 and AP1 proteins, and to a much lesser extent Gfi1 and C/EBPa (Fig. 6A). To better  
169 understand which connections involving the PU.1 and AP1 proteins were important, we  
170 simulated the pairwise deletion of interactions between these proteins and their respective  
171 regulatory targets. SVD decomposition of the state displacement matrix assembled from  
172 the pairwise deletion of interactions, suggested the first five modes accounted for >99%  
173 of the variance resulting from deletion of the interactions. The most sensitive interactions  
174 for the PU.1 protein involved the C/EBPa-dependent regulation of P47Phox expression,

and to a lesser extent AP1 and EGR1 expression (Fig. 6B). On the other other, the most sensitive connections for AP1 involved the C/EBPa-dependent regulation of p21 expression, and the mutual activation of PU.1 and AP1 expression. Taken together, these results suggested that the PU.1 and AP1 proteins acted as important self-reinforcing regulators for both the signal integration and phenotype modules. The analysis suggested that the PU.1 signaling axis promoted the formation of the neutrophil NADPH oxidase (through p47Phox), while AP1 was responsible for cell cycle arrest (through p21). However, this analysis did not give insight into which upstream components of the signal initiation module were important. Toward this question, we explored the composition and regulation of the signalsome complex by experimentally interrogating a panel of possible Raf interaction partners.

The composition of the signalsome, and the kinase ultimately responsible for mediating ATRA-induced Raf activation is currently unknown. To explore this question, we conducted immunoprecipitation and subsequent Western blotting to identify physical interactions between Raf and 19 putative interaction partners. A panel of 19 possible Raf interaction partners (kinases, GTPases, scaffolding proteins etc) was constructed based upon known signaling pathways. We did not consider the most likely binding partner, the small GTPase RAS, as previous studies have ruled it out in MAPK activation in HL-60 cells (20, 27). Total Raf was used as a bait protein for the immunoprecipitation studies. Interrogation of the Raf interactome suggested Vav1 was involved with ATRA-induced initiation of MAPK activity (Fig. 7). Western blot analysis using total Raf and pS621 Raf specific antibodies confirmed the presence of the bait protein, total and phosphorylated forms, in the immunoprecipitate (Fig. 7A). Of the 19 proteins sampled, Vav1, Src, CK2, Akt, and 14-3-3 precipitated with Raf, suggesting a direct physical interaction was possible. However, only the associations between Raf and Vav1 and Raf and Src were ATRA-inducible (Fig. 7). Furthermore, the Vav1 and Src associations were correlated with pS621 Raf

abundance in the precipitate. Others proteins e.g., CK2, Akt and 14-3-3, generally bound Raf regardless of phosphorylation status or ATRA treatment. The remaining 14 proteins were expressed in whole cell lysate (Fig. 7B), but were not detectable in the precipitate of Raf IP. Treatment with the Raf kinase inhibitor GW5074 following ATRA exposure reduced the association of both Vav1 with Raf and Src with Raf (Fig. 7), although the signal intensity for Src was notably weak. However, GW5074 did not influence the association of CK2 or 14-3-3 with Raf, further demonstrating their independence from Raf phosphorylation. Interestingly, the Raf-Akt interaction qualitatively increased following treatment with GW5074; however, it remained unaffected by treatment with ATRA. Src family kinases are known to be important in myeloid differentiation (28) and their role in HL-60 differentiation has been investigated elsewhere (11). Given the existing work and variable reproducibility in the context of the Raf immunoprecipitate, we did not investigate the role of Src further in this study. Taken together, the immunoprecipitation and GW5074 results implicated Vav1 association to be correlated with Raf activation following ATRA-treatment. Previous studies demonstrated that a Vav1-Slp76-Cbl-CD38 complex plays an important role in ATRA-induced MAPK activation and differentiation of HL-60 cells (13). Here we did not observe direct interaction of Raf with Cbl or Slp76; however, this complex could be involved upstream. Next, we considered the effect of the Raf kinase inhibitor GW5074 on functional markers of ATRA-induced growth arrest and differentiation.

Inhibition of Raf kinase activity modulated MAPK activation and differentiation markers following ATRA exposure (Fig. 7D-F). ATRA treatment alone statistically significantly increased the G1/G0 percentage over the untreated control, while GW5074 alone had a negligible effect on the cell cycle distribution (Fig. 7D). Surprisingly, the combination of GW5074 and ATRA statistically significantly increased the G1/G0 population ( $82 \pm 1\%$ ) compared with ATRA alone ( $61 \pm 0.5\%$ ). Increased G1/G0 arrest following the combined treatment with GW5074 and ATRA was unexpected, as the combination of ATRA and the

227 MEK inhibitor (PD98059) has been shown previously to decrease ATRA-induced growth  
228 arrest (8). However, growth arrest is not the sole indication of functional differentiation.  
229 Expression of the cell surface marker CD11b has also been shown to coincide with HL-60  
230 cells myeloid differentiation (29). We measured CD11b expression, for the various treat-  
231 ment groups, using immuno-fluorescence flow cytometry 48 hr post-treatment. As with  
232 G1/G0 arrest, ATRA alone increased CD11b expression over the untreated control, while  
233 GW5074 further enhanced ATRA-induced CD11b expression (Fig. 7E). GW5074 alone  
234 had no statistically significant effect on CD11b expression, compared with the untreated  
235 control. Lastly, the inducible reactive oxygen species (ROS) response was used as a func-  
236 tional marker of differentiated neutrophils (16). We measured the ROS response induced  
237 by the phorbol ester 12-O-tetradecanoylphorbol-13-acetate (TPA) using flow cytometry.  
238 Untreated cells showed no discernible TPA response, with only  $7.0 \pm 3.0\%$  ROS induction  
239 (Fig. 7F). Cells treated with ATRA had a significantly increased TPA response,  $53 \pm 7\%$   
240 ROS induction 48 hr post-treatment. Treatment with both ATRA and GW5074 statistically  
241 significantly reduced ROS induction ( $22 \pm 0.6\%$ ) compared to ATRA alone. Interestingly,  
242 Western blot analysis did not detect a GW5074 effect on ATRA-induced expression of  
243 p47phox, a required upstream component of the ROS response (Fig. 7F, bottom). Thus,  
244 the inhibitory effect of GW5074 on inducible ROS might occur downstream of p47phox  
245 expression. However, the ROS producing complex is MAPK dependent, therefore it is  
246 also possible that GW5074 inhibited ROS production by interfering with MAPK activation  
247 (in which case the p47Phox marker might not accurately reflect phenotypic conversion  
248 and differentiation).

249 **Discussion**

250 In this study, we presented an effective model of ATRA-inducible differentiation of HL-60  
251 cells which encoded positive feedback between the ATRA-inducible signalsome complex  
252 and the MAPK pathway. Despite its simplicity, the model captured key features of the  
253 ATRA induced differentiation such as sustained MAPK activation, and bistability with re-  
254 spect to ATRA exposure. We also reported a new ATRA-inducible component of the  
255 signalsome, Vav1. Vav1 is a guanine nucleotide exchange factor for Rho family GTPases  
256 that activate pathways leading to actin cytoskeletal rearrangements and transcriptional al-  
257 terations (30). The Vav1/Raf association correlated with Raf activity, was ATRA-inducible  
258 and decreased after treatment with GW5074. The presence of Vav1 in Raf/Grb2 com-  
259 plexes has been shown to correlate with increased Raf activity in mast cells (31). Fur-  
260 thermore, studies on Vav1 knockout mice demonstrated that the loss of Vav1 resulted  
261 in deficiencies of ERK signaling for both T-cells as well as neutrophils (32, 33). While its  
262 function in the signalsome is unclear, Vav1 has been shown to associate with a Cbl-Slp76-  
263 CD38 complex in an ATRA-dependent manner; furthermore, transfection of HL-60 cells  
264 with Cbl mutants that fail to bind CD38, yet still bind Slp76 and Vav1, prevented ATRA-  
265 induced MAPK activation (13). Thus, interaction of Cbl-Slp76-Vav1 and CD38 appears to  
266 be required for transmission of the ATRA signal by the signalsome.

267 Analysis of the signal integration and phenotype modules suggested that PU.1 and  
268 AP1 regulated distinct phenotypic axes following ATRA exposure.

269 Immunoprecipitation studies identified a limited number of ATRA-dependent and -  
270 independent Raf interaction partners. While we were unable to detect the association  
271 of Raf with common kinases and GTPases such as PKC, PKA, p38, Rac and Rho, we  
272 did establish potential interactions between Raf and key partners such as Vav1, Src, Akt,  
273 CK2 and 14-3-3. All of these partners are known to be associated with Raf activation  
274 or function. Src is known to bind Raf through an SH2 domain, and this association has

been shown to be dependent of the serine phosphorylation of Raf (34). Thus, an ATRA inducible Src/Raf association may be a result of ATRA-induced Raf phosphorylation at S259 or S621. We also identified an interaction between Raf and the Ser/Thr kinases Akt and CK2. Akt can phosphorylate Raf at S259, as demonstrated by studies in a human breast cancer line (35). CK2 can also phosphorylate Raf, although the literature has traditionally focused on S338 and not S621 or S259(36). However, neither of these kinase interactions were ATRA-inducible, suggesting their association with Raf alone was not associated with ATRA-induced Raf phosphorylation. The adapter protein 14-3-3 was also constitutively associated with Raf. The interaction between Raf and 14-3-3 has been associated with both S621 and S259 phosphorylation and activity (37). Additionally, the association of Raf with 14-3-3 not only stabilized S621 phosphorylation, but also reversed the S621 phosphorylation from inhibitory to activating (38). Finally, we found that Vav1/Raf association correlated with Raf activity, was ATRA-inducible and decreased after treatment with GW5074. The presence of Vav1 in Raf/Grb2 complexes has been shown to correlate with increased Raf activity in mast cells (31). Furthermore, studies on Vav1 knockout mice demonstrated that the loss of Vav1 resulted in deficiencies of ERK signaling for both T-cells as well as neutrophils (32, 33). Interestingly, while an integrin ligand-induced ROS response was blocked in Vav1 knockout neutrophils, TPA was able to bypass the Vav1 requirement and stimulate both ERK phosphorylation and ROS induction (33). In this study, the TPA-induced ROS response was dependent upon Raf kinase activity, and was mitigated by the addition of GW5074. It is possible that Vav1 is downstream of various integrin receptors but upstream of Raf in terms of inducible ROS responses. Vav1 has also been shown to associate with a Cbl-Slp76-CD38 complex in an ATRA-dependent manner; furthermore, transfection of HL-60 cells with Cbl mutants that fail to bind CD38, yet still bind Slp76 and Vav1, prevents ATRA-induced MAPK activation (13). The literature suggest a variety of possible receptor-signaling pathways, which involve Vav1, for MAPK

301 activation; moreover, given the ATRA-inducible association Vav1 may play a direct role in  
302 Raf activation.

303 We hypothesized that Vav1 is a member of an ATRA-inducible complex which propels  
304 sustained MAPK activation, arrest and differentiation. Initially, ATRA-induced Vav1 ex-  
305 pression drives increased association between Vav1 and Raf. This increased interaction  
306 facilitates phosphorylation and activation of Raf by pre-bound Akt and/or CK2 at S621  
307 or perhaps S259. Constitutively bound 14-3-3 may also stabilize the S621 phosphory-  
308 lation, modulate the activity and/or up-regulate autophosphorylation. Activated Raf can  
309 then drive ERK activation, which in turn closes the positive feedback loop by activating  
310 Raf transcription factors, e.g. Sp1 and/or STAT1 (39–42). We tested this working hy-  
311 pothesis using mathematical modeling. The model recapitulated both ATRA time-course  
312 data as well as the GW5074 inhibitor effects. This suggested the proposed Raf-Vav1  
313 architecture was at least consistent with the experimental studies. Further, analysis of  
314 the Raf-Vav1 model identified bistability in ppERK levels. Thus, two possible MAPK ac-  
315 tivation branches were possible for experimentally testable ATRA values. The analysis  
316 also suggested the ATRA-induced Raf-Vav1 architecture could be locked into a sustained  
317 signaling mode (high ppERK) even in the absence of a ATRA signal. This locked-in prop-  
318 erty could give rise to an ATRA-induction memory. We validated the treatment memory  
319 property predicted by the Raf-Vav1 circuit experimentally using ATRA-washout experi-  
320 ments. ERK phosphorylation levels remained high for more then 96 hr after ATRA was  
321 removed. Previous studies demonstrated that HL-60 cells possessed an inheritable mem-  
322 ory of ATRA stimulus (43). Although the active state was self-sustaining, the inactive state  
323 demonstrated considerable robustness to perturbation. For example, we found that 50x  
324 overexpression of Raf was required to reliably lock MAPK into the activated state, while  
325 small perturbations had almost no effect on ppERK levels over the entire ensemble. CD38  
326 expression correlated with the ppERK, suggesting its involvement in the signaling com-

327 plex. Our computational and experimental results showed that positive feedback, through  
328 ERK-dependent Raf expression, could sustain MAPK signaling through many division cy-  
329 cles. Such molecular mechanisms could underly aspects of cellular memory associated  
330 to consecutive ATRA treatments.

331 Several engineered, or naturally occurring systems involved in cell fate decisions incor-  
332 porate positive feedback and bistability (44). One of the most well studied cell fate circuits  
333 is the Mos mitogen-activated protein kinase cascade in *Xenopus* oocytes. This cascade  
334 is activated when oocytes are induced by the steroid hormone progesterone (45). The  
335 MEK-dependent activation of p42 MAPK stimulates the accumulation of the Mos onco-  
336 protein, which in turn activates MEK, thereby closing the feedback loop. This is similar to  
337 the differentiation circuit presented here; ATRA drives signalsome which activates MAPK,  
338 cell-cycle arrest, differentiation and signalsome. Thus, while HL-60 and *Xenopus* oocytes  
339 are vastly different biological models, they share similar cell fate decision architectures.  
340 Other unrelated cell fate decisions such as programmed cell death have also been sug-  
341 gested to be bistable (46). Still more biochemical networks important to human health,  
342 for example the human coagulation or complement cascades, also feature strong positive  
343 feedback elements (47). Thus, while positive feedback is sometimes not desirable in man-  
344 made systems, it may be at the core of a diverse variety of cell fate programs and other  
345 networks important to human health.

346 Model performance was impressive given its limited size. However, there were several  
347 issues to explore further. First, there was likely missing connectivity in the effective differ-  
348 entiation circuit. Decreasing BLR1 expression with simultaneously sustained cRaf-pS261  
349 activation was not captured by the current network architecture. This suggested that  
350 signalsome, once activated, had a long lifetime as decreased BLR1 expression did not  
351 impact cRaf-pS261 abundance. We could model this by separating signalsome formation  
352 into an inactive precursor pool that is transformed to a long-lived activated signalsome by

353 MAPK activation. We should also explore adding additional downstream biological mod-  
354 ules to this skeleton model, for example the upregulation of reactive oxygen markers such  
355 as p47Phox or cell cycle arrest components to capture the switch from an actively prolif-  
356 erating population to a population in G0-arrest. Next, the choice of max/min integration  
357 rules or the particular form of the transfer functions could also be explored. Integration  
358 rules other than max/min could be used, such as the mean or the product, assuming the  
359 range of the transfer functions is always  $f \in [0, 1]$ . Alternative integration rules might  
360 have different properties which could influence model identification or performance. For  
361 example, a mean integration rule would be differentiable, allowing derivative-based opti-  
362 mization approaches to be used. The form of the transfer function could also be explored.  
363 We choose hill-like functions because of their prominence in the systems and synthetic  
364 biology community. However, many other transfer functions are possible.

365 **Materials and Methods**

366 *Effective gene expression model equations.* We decomposed the ATRA-induced differ-  
 367 entiation program into three modules; a signal initiation module that sensed and trans-  
 368 formed the ATRA signal into activated cRaf-pS621 and the ATRA-RXR/RAR (activated  
 369 Trigger) signals; a signal integration module that controlled the expression of upstream  
 370 transcription factors given cRaf-pS621 and activated Trigger signals; and a phenotype  
 371 module which encoded the expression of functional differentiation markers from the ATRA-  
 372 inducible transcription factors. The output of the signal initiation module was the input to  
 373 the gene expression model. For each gene  $j = 1, 2, \dots, \mathcal{G}$ , we modeled both the mRNA  
 374 ( $m_j$ ), protein ( $p_j$ ) and signaling species abundance:

$$\frac{dm_j}{dt} = r_{T,j} - (\mu + \theta_{m,j}) m_j + \lambda_j \quad (1)$$

$$\frac{dp_j}{dt} = r_{X,j} - (\mu + \theta_{p,j}) p_j \quad (2)$$

$$g(p_1, \dots, p_{\mathcal{G}}, \kappa) = 0 \quad (3)$$

375 The terms  $r_{T,j}$  and  $r_{X,j}$  denote the specific rates of transcription, and translation while  
 376 the terms  $\theta_{m,j}$  and  $\theta_{p,j}$  denote first-order degradation constants for mRNA and protein,  
 377 respectively. The specific transcription rate  $r_{T,j}$  was modeled as the product of a kinetic  
 378 term  $\bar{r}_{T,j}$  and a control term  $u_j$  which described how the abundance of transcription fac-  
 379 tors, or other regulators influenced the expression of gene  $j$ . The kinetic transcription  
 380 term  $\bar{r}_{T,j}$  was modeled as:

$$\bar{r}_{T,j} = V_T^{max} \left( \frac{L_{T,o}}{L_{T,j}} \right) \left( \frac{G_j}{K_T + G_j} \right) \quad (4)$$

381 where the maximum gene expression rate  $V_T^{max}$  was defined as the product of a char-  
 382 acteristic transcription rate constant ( $k_T$ ) and the abundance of RNA polymerase ( $R_1$ ),

383  $V_T^{max} = k_T(R_1)$ . The  $(L_{T,o}/L_{T,j})$  term denotes the ratio of transcription read lengths;  $L_{T,o}$   
 384 represents a characteristic gene length, while  $L_{T,j}$  denotes the length of gene  $j$ . Thus,  
 385 the ratio  $(L_{T,o}/L_{T,j})$  is a gene specific correction to the characteristic transcription rate  
 386  $V_T^{max}$ . The degradation rate constants were defined as  $\theta_{m,j}$  and  $\theta_{p,j}$  denote characteristic  
 387 degradation constants for mRNA and protein, respectively. Lastly, the  $\lambda_j$  term denotes the  
 388 constitutive rate of expression of gene  $j$ .

389 The gene expression control term  $0 \leq u_j \leq 1$  depended upon the combination of fac-  
 390 tors which influenced the expression of gene  $j$ . If the expression of gene  $j$  was influenced  
 391 by  $1, \dots, m$  factors, we modeled this relationship as  $u_j = \mathcal{I}_j(f_{1j}(\cdot), \dots, f_{mj}(\cdot))$  where  
 392  $0 \leq f_{ij}(\cdot) \leq 1$  denotes a regulatory transfer function quantifying the influence of factor  $i$   
 393 on the expression of gene  $j$ , and  $\mathcal{I}_j(\cdot)$  denotes an integration rule which combines the  
 394 individual regulatory inputs for gene  $j$  into a single control term. In this study, the integra-  
 395 tion rule governing gene expression was the weighted fraction of promoter configurations  
 396 that resulted in gene expression (48):

$$u_j = \frac{W_{R_{1,j}} + \sum_n W_{nj} f_{nj}}{1 + W_{R_{1,j}} + \sum_d W_{dj} f_{dj}} \quad (5)$$

397 The numerator, the weighted sum (with weights  $W_{nj}$ ) of promoter configurations leading to  
 398 gene expression, was normalized by all possible promoter configurations. The likelihood  
 399 of each configuration was quantified by the transfer function  $f_{nj}$  (which we modeled using  
 400 hill like functions), while the lead term in the numerator  $W_{R_{1,j}}$  denotes the weight of con-  
 401 stitutive expression for gene  $j$ . Given this formulation, the rate of constitutive expression  
 402 was then given by:

$$\lambda_j = \bar{r}_{T,j} \left( \frac{W_{R_{1,j}}}{1 + W_{R_{1,j}}} \right) \quad (6)$$

403 If a gene expression process had no modifying factors,  $u_j = 1$ . Lastly, the specific trans-

404 lation rate was modeled as:

$$r_{X,j} = V_X^{\max} \left( \frac{L_{X,o}}{L_{X,j}} \right) \left( \frac{m_j}{K_X + m_j} \right) \quad (7)$$

405 where  $V_X^{\max}$  denotes a characteristic maximum translation rate estimated from literature,  
406 and  $K_X$  denotes a translation saturation constant. The characteristic maximum translation  
407 rate was defined as the product of a characteristic translation rate constant ( $k_X$ ) and  
408 the Ribosome abundance ( $R_2$ ),  $V_X^{\max} = k_X (R_2)$ . As was the case for transcription, we  
409 corrected the characteristic translation rate by the ratio of the length of a characteristic  
410 transcription normalized by the length of transcript  $j$ .

411 *Signaling model equations.* The signal initiation, and integration modules required the  
412 abundance of cRaf-pS621 and ATRA-RXR/RAR (activated Trigger) as inputs. However,  
413 our base model described only the abundance of inactive proteins e.g., cRaf or RXR/RAR  
414 but not the activated forms. To address this issue, we estimated pseudo steady state  
415 approximations for the abundance of cRaf-pS621 and activated Trigger (shown generally  
416 as Eq (3)). The abundance of activated trigger ( $x_{a,1}$ ) was estimated directly from the  
417 RXR/RAR abundance ( $x_{u,1}$ ):

$$x_{a,1} \sim x_{u,1} \left( \frac{\alpha \cdot \text{ATRA}}{1 + \alpha \cdot \text{ATRA}} \right) \quad (8)$$

418 where  $\alpha$  denotes a gain parameter;  $\alpha = 0.0$  if ATRA is less than a threshold, and  $\alpha = 0.1$   
419 if ATRA is greater than the differentiation threshold. The abundance of cRaf-pS621 was  
420 estimated by making the pseudo steady state approximation on the cRaf-pS621 balance.  
421 The abundance of an activated signaling species  $i$  was given by:

$$\frac{dx_i}{dt} = r_{+,i}(\mathbf{x}, \mathbf{k}) - (\mu + k_{d,i}) x_i \quad i = 1, \dots, \mathcal{M} \quad (9)$$

422 The quantity  $x_i$  denotes concentration of signaling species  $i$ , while  $\mathcal{R}$  and  $\mathcal{M}$  denote  
 423 the number of signaling reactions and signaling species in the model, respectively. The  
 424 term  $r_{+,i}(\mathbf{x}, \mathbf{k})$  denotes the rate of generation of activated species  $i$ , while  $\mu$  denotes  
 425 the specific growth rate, and  $k_{d,i}$  denotes the rate constant controlling the non-specific  
 426 degradation of  $x_i$ . We neglected deactivation reactions e.g., phosphatase activities. We  
 427 assumed that signaling processes were fast compared to gene expression; this allowed  
 428 us to approximate the signaling balance as:

$$x_i^* \simeq \frac{r_{+,i}(\mathbf{x}, \mathbf{k})}{(\mu + k_{d,i})} \quad i = 1, \dots, \mathcal{M} \quad (10)$$

429 The generation rate was written as the product of a kinetic term ( $\bar{r}_{+,i}$ ) and a control term  
 430 ( $v_i$ ). The control terms  $0 \leq v_j \leq 1$  depended upon the combination of factors which in-  
 431 fluenced rate process  $j$ . If rate  $j$  was influenced by  $1, \dots, m$  factors, we modeled this  
 432 relationship as  $v_j = \mathcal{I}_j(f_{1j}(\cdot), \dots, f_{mj}(\cdot))$  where  $0 \leq f_{ij}(\cdot) \leq 1$  denotes a regulatory  
 433 transfer function quantifying the influence of factor  $i$  on rate  $j$ . The function  $\mathcal{I}_j(\cdot)$  is an  
 434 integration rule which maps the output of regulatory transfer functions into a control vari-  
 435 able. In this study, we used  $\mathcal{I}_j \in \{\min, \max\}$  and hill transfer functions (49). If a process  
 436 had no modifying factors,  $v_j = 1$ . The kinetic rate of cRaf-pS621 generation  $\bar{r}_{+,cRaf}$  was  
 437 modeled as:

$$\bar{r}_{+,cRaf} = k_{+,cRaf} x_s \left( \frac{x_{cRaf}}{K_{+,cRaf} + x_{cRaf}} \right) \quad (11)$$

438 where  $x_s$  denotes the signalsome abundance, and  $K_{+,cRaf}$  denotes a saturation constant  
 439 governing cRaf-pS621 formation. The formation of cRaf-pS621 was regulated by only a  
 440 single factor, the abundance of MAPK inhibitor, thus  $v_{+,cRaf}$  took the form:

$$v_{+,cRaf} = \left( 1 - \frac{I}{K_D + I} \right) \quad (12)$$

441 where  $I$  denotes the abundance of the MAPK inhibitor, and  $K_D$  denotes the inhibitor  
442 affinity.

443 *Estimation of gene expression model parameters.* We estimated parameters appearing  
444 in the mRNA and protein balances, the abundance of polymerases and ribosomes, tran-  
445 scription and translation rates, the half-life of a typical mRNA and protein, and typical  
446 values for the copies per cell of RNA polymerase and ribosomes from literature (Table 2).  
447 The saturation constants  $K_X$  and  $K_T$  were adjusted so that gene expression and trans-  
448 lation resulted in gene products on a biologically realistic concentration scale. Lastly, we  
449 calculated the concentration for gene  $G_j$  by assuming, on average, that a cell had two  
450 copies of each gene at any given time. Thus, the bulk of our gene expression model pa-  
451 rameters were based directly upon literature values, and were not adjusted during model  
452 identification. However, the remaining parameters, e.g., the  $W_{ij}$  appearing in the gene  
453 expression control laws, or parameters appearing in the transfer functions  $f_{dij}$ , were esti-  
454 mated from the protein expression and signaling data sets discussed here.

455 Signaling and gene expression model parameters were estimated by minimizing the  
456 squared difference between simulations and experimental protein data set  $j$ . We mea-  
457 sured the squared difference in the scale, fold change and shape for protein  $j$ :

$$E_j(\mathbf{k}) = \left( \mathcal{M}_j(t_-) - \hat{y}_j(t_-, \mathbf{k}) \right)^2 + \sum_{i=1}^{\mathcal{T}_j} \left( \hat{\mathcal{M}}_{ij} - \hat{y}_{ij}(\mathbf{k}) \right)^2 + \sum_{i=1}^{\mathcal{T}_j} \left( \mathcal{M}'_{ij} - y'_{ij}(\mathbf{k}) \right)^2 \quad (13)$$

458 The first term in Eqn. (13) quantified the initial *scale* error, directly before the addition  
459 of ATRA. In this case,  $\mathcal{M}_j(t_-)$  (the approximate concentration of protein  $j$  before the  
460 addition of ATRA) was estimated from literature. This term was required because the  
461 protein measurements were reported as the fold-change; thus, the data was normalized  
462 by a control value measured before the addition of ATRA. However, the model operated on  
463 a physical scale. The first term allowed the model to capture physically realistic changes

464 following ATRA addition. The second term quantified the difference in the *fold-change* of  
 465 protein  $j$  as a function of time. The terms  $\hat{\mathcal{M}}_{ij}$  and  $\hat{y}_{ij}$  denote the scaled experimental  
 466 observations and simulation outputs (fold-change; protein normalized by control value  
 467 directly before ATRA addition) at time  $i$  from protein  $j$ , where  $T_j$  denoted the number of  
 468 time points for data set  $j$ . Lastly, the third term of the objective function measured the  
 469 difference in the *shape* of the measured and simulated protein levels. The scaled value  
 470  $0 \leq \mathcal{M}'_{ij} \leq 1$  was given by:

$$\hat{\mathcal{M}}_{ij} = \left( \mathcal{M}_{ij} - \min_i \mathcal{M}_{ij} \right) / \left( \max_i \mathcal{M}_{ij} - \min_i \mathcal{M}_{ij} \right) \quad (14)$$

471 where  $\mathcal{M}'_{ij} = 0$  and  $\mathcal{M}'_{ij} = 1$  describe the lowest (highest) intensity bands. A similar  
 472 scaling was used for the simulation output. We minimized the total model residual  $\sum_j E_j$   
 473 using a heuristic direct-search optimization procedure, subject to box constraints on the  
 474 parameter values, starting from a random initial parameter guess. Each downhill step was  
 475 archived and used for ensemble calculations. The optimization procedure (a covariance  
 476 matrix adaptation evolution strategy) has been reported previously (50).

477 *Estimation of an effective cell cycle arrest model.* We formulated an effective N-order  
 478 polynomial model of the fraction of cells undergoing ATRA-induced cell cycle arrest at  
 479 time  $t$ ,  $\hat{\mathcal{A}}(t)$ , as:

$$\hat{\mathcal{A}}(t) \simeq a_0 + \sum_{i=1}^{N-1} a_i \phi_i(\mathbf{p}(t), t) \quad (15)$$

480 where  $a_i$  were unknown parameters, and  $\phi_i(\mathbf{p}(t), t)$  denotes a basis function. The basis  
 481 functions were dependent upon the system state; in this study, we assumed  $N = 4$  and  
 482 basis functions of the form:

$$\phi_i(\mathbf{p}(t), t) = \left( \frac{t}{T} + \frac{p21}{E2F} \Big|_t \right)^{(i-1)} \quad (16)$$

483 The parameters  $a_0, \dots, a_3$  were estimated directly from cell-cycle measurements (biologi-  
484 cal replicates) using least-squares.

485 *Availability of model code.* The signaling and gene expression model equations, and the  
486 parameter estimation procedure, were implemented in the Julia programming language.  
487 The model equations were solved using the ODE23s routine of the ODE package (51). The  
488 model code and parameter ensemble is freely available under an MIT software license  
489 and can be downloaded from <http://www.varnerlab.org>.

490 *Cell culture and treatment* Human myeloblastic leukemia cells (HL-60 cells) were grown  
491 in a humidified atmosphere of 5% CO<sub>2</sub> at 37°C and maintained in RPMI 1640 from Gibco  
492 (Carlsbad, CA) supplemented with 5% heat inactivated fetal bovine serum from Hyclone  
493 (Logan, UT) and 1× antibiotic/antimicotic (Gibco, Carlsbad, CA). Cells were cultured in  
494 constant exponential growth (52). Experimental cultures were initiated at  $0.1 \times 10^6$  cells/mL  
495 24 hr prior to ATRA treatment; if indicated, cells were also treated with GW5074 (2 $\mu$ M) 18  
496 hr before ATRA treatment. For the cell culture washout experiments, cells were treated  
497 with ATRA for 24 hr, washed 3x with prewarmed serum supplemented culture medium  
498 to remove ATRA, and reseeded in ATRA-free media as described. Western blot analysis  
499 was performed at incremental time points after removal of ATRA.

500 *Chemicals* All-Trans Retinoic Acid (ATRA) from Sigma-Aldrich (St. Louis, MO) was dis-  
501 solved in 100% ethanol with a stock concentration of 5mM, and used at a final concen-  
502 tration of 1 $\mu$ M (unless otherwise noted). The cRaf inhibitor GW5074 from Sigma-Aldrich  
503 (St. Louis, MO) was dissolved in DMSO with a stock concentration of 10mM, and used  
504 at a final concentration of 2 $\mu$ M. HL-60 cells were treated with 2 $\mu$ M GW5074 with or with-  
505 out ATRA (1 $\mu$ M) at 0 hr. This GW5074 dosage had a negligible effect on the cell cycle  
506 distribution, compared to ATRA treatment alone.

507 *Immunoprecipitation and western blotting* Approximately  $1.2 \times 10^7$  cells were lysed using  
508  $400\mu\text{L}$  of M-Per lysis buffer from Thermo Scientific (Waltham, MA). Lysates were cleared  
509 by centrifugation at  $16,950 \times g$  in a micro-centrifuge for 20 min at  $4^\circ\text{C}$ . Lysates were  
510 pre-cleared using  $100\mu\text{L}$  protein A/G Plus agarose beads from Santa Cruz Biotechnology  
511 (Santa Cruz, CA) by inverting overnight at  $4^\circ\text{C}$ . Beads were cleared by centrifugation and  
512 total protein concentration was determined by a BCA assay (Thermo Scientific, Waltham,  
513 MA). Immunoprecipitations were setup by bringing lysate to a concentration of 1g/L in a  
514 total volume of  $300\mu\text{L}$  (M-Per buffer was used for dilution). The anti-Raf antibody was  
515 added at  $3\mu\text{L}$ . A negative control with no bait protein was also used to exclude the di-  
516 rect interaction of proteins with the A/G beads. After 1 hr of inversion at  $4^\circ\text{C}$ ,  $20\mu\text{L}$  of  
517 agarose beads was added and samples were left to invert overnight at  $4^\circ\text{C}$ . Samples  
518 were then washed three times with M-Per buffer by centrifugation. Finally proteins were  
519 eluted from agarose beads using a laemmli loading buffer. Eluted proteins were resolved  
520 by SDS-PAGE and Western blotting. Total lysate samples were normalized by total protein  
521 concentration ( $20\mu\text{g}$  per sample) and resolved by SDS-PAGE and Western blotting. Sec-  
522 ondary HRP bound antibody was used for visualization. All antibodies were purchased  
523 from Cell Signaling (Boston, MA) with the exception of  $\alpha$ -p621 Raf which was purchased  
524 from Biosource/Invitrogen (Carlsbad, CA), and  $\alpha$ -CK2 from BD Biosciences (San Jose,  
525 CA).

526 *Morphology assessment* Untreated and ATRA-treated HL-60 cells were collected after  
527 72 hr and cytocentrifuged for 3 min at 700 rpm onto glass slides. Slides were air-dried  
528 and stained with Wright's stain. Slide images were captured at 40X (Leica DM LB 100T  
529 microscope, Leica Microsystems).

530 **Competing interests**

531 The authors declare that they have no competing interests.

532 **Author's contributions**

533 J.V and A.Y directed the study. R.T, H.J, R.B and J.C conducted the cell culture measure-  
534 ments. J.V, R.B, W.D, K.R and A.S developed the reduced order HL-60 models and the  
535 parameter ensemble. W.D and J.V analyzed the model ensemble, and generated figures  
536 for the manuscript. The manuscript was prepared and edited for publication by W.D, A.Y  
537 and J.V.

538 **Acknowledgements**

539 We gratefully acknowledge the suggestions from the anonymous reviewers to improve  
540 this manuscript.

541 **Funding**

542 We acknowledge the financial support to J.V. by the National Science Foundation CA-  
543 REER (CBET-0846876) for the support of R.T. and H.J. In addition, we acknowledge  
544 support to A.Y. from the National Institutes of Health (CA 30555, CA152870) and a grant  
545 from New York State Stem Cell Science. Lastly, we acknowledge the financial support to  
546 J.V. and A.Y. from the National Cancer Institute (#U54 CA143876). The content is solely  
547 the responsibility of the authors and does not necessarily represent the official views of  
548 the National Cancer Institute or the National Institutes of Health.

549 **References**

- 550 1. Bushue N, Wan YJY (2010) Retinoid pathway and cancer therapeutics. *Adv Drug  
551 Deliv Rev* 62: 1285-98.
- 552 2. Tang XH, Gudas LJ (2011) Retinoids, retinoic acid receptors, and cancer. *Annu Rev  
553 Pathol* 6: 345-64.
- 554 3. Cheung FSG, Lovicu FJ, Reichardt JKV (2012) Current progress in using vitamin d  
555 and its analogs for cancer prevention and treatment. *Expert Rev Anticancer Ther*  
556 12: 811-37.
- 557 4. Nilsson B (1984) Probable in vivo induction of differentiation by retinoic acid of  
558 promyelocytes in acute promyelocytic leukaemia. *Br J Haematol* 57: 365-71.
- 559 5. Warrell RP Jr (1993) Retinoid resistance in acute promyelocytic leukemia: new  
560 mechanisms, strategies, and implications. *Blood* 82: 1949-53.
- 561 6. Freemantle SJ, Spinella MJ, Dmitrovsky E (2003) Retinoids in cancer therapy and  
562 chemoprevention: promise meets resistance. *Oncogene* 22: 7305-15.
- 563 7. Breitman TR, Selonick SE, Collins SJ (1980) Induction of differentiation of the hu-  
564 man promyelocytic leukemia cell line (HL-60) by retinoic acid. *Proc Natl Acad Sci U  
565 S A* 77: 2936–2940.
- 566 8. Yen A, Roberson MS, Varvayanis S, Lee AT (1998) Retinoic acid induced  
567 mitogen-activated protein (MAP)/extracellular signal-regulated kinase (ERK) kinase-  
568 dependent MAP kinase activation needed to elicit HL-60 cell differentiation and  
569 growth arrest. *Cancer Res* 58: 3163–3172.
- 570 9. Hong HY, Varvayanis S, Yen A (2001) Retinoic acid causes MEK-dependent RAF  
571 phosphorylation through RARalpha plus RXR activation in HL-60 cells. *Differentia-  
572 tion* 68: 55–66.
- 573 10. Mangelsdorf DJ, Ong ES, Dyck JA, Evans RM (1990) Nuclear receptor that identifies  
574 a novel retinoic acid response pathway. *Nature* 345: 224–229.

- 575 11. Congleton J, MacDonald R, Yen A (2012) Src inhibitors, PP2 and dasatinib, increase  
576 retinoic acid-induced association of Lyn and c-Raf (S259) and enhance MAPK-  
577 dependent differentiation of myeloid leukemia cells. Leukemia 26: 1180-8.
- 578 12. Shen M, Bunaci R, Congleton J, Jensen H, Sayam L, et al. (2011) Interferon regu-  
579 latory factor-1 binds c-Cbl, enhances mitogen activated protein kinase signaling and  
580 promotes retinoic acid-induced differentiation of HL-60 human myelo-monoblastic  
581 leukemia cells. Leuk Lymphoma 52: 2372-9.
- 582 13. Shen M, Yen A (2009) c-Cbl tyrosine kinase-binding domain mutant G306E abol-  
583 ishes the interaction of c-Cbl with CD38 and fails to promote retinoic acid-induced  
584 cell differentiation and G0 arrest. J Biol Chem 284: 25664–25677.
- 585 14. Yen A, Varvayanis S, Smith J, Lamkin T (2006) Retinoic acid induces expression of  
586 SLP-76: expression with c-FMS enhances ERK activation and retinoic acid-induced  
587 differentiation/G0 arrest of HL-60 cells. Eur J Cell Biol 85: 117–132.
- 588 15. Marchisio M, Bertagnolo V, Colamussi ML, Capitani S, Neri LM (1998) Phos-  
589 phatidylinositol 3-kinase in HL-60 nuclei is bound to the nuclear matrix and increases  
590 during granulocytic differentiation. Biochem Biophys Res Commun 253: 346-51.
- 591 16. Congleton J, Jiang H, Malavasi F, Lin H, Yen A (2011) ATRA-induced HL-60 myeloid  
592 leukemia cell differentiation depends on the CD38 cytosolic tail needed for mem-  
593 brane localization, but CD38 enzymatic activity is unnecessary. Exp Cell Res 317:  
594 910–919.
- 595 17. Wang J, Yen A (2004) A novel retinoic acid-responsive element regulates retinoic  
596 acid induced BLR1 expression. Mol Cell Biol 24: 2423 - 2443.
- 597 18. Yen A (1990) HL-60 cells as a model of growth and differentiation: the significance  
598 of variant cells. Hematology Review 4: 5-46.
- 599 19. Yang T, Xiong Q, Enslen H, Davis R, Chow CW (2002) Phosphorylation of NFATc4  
600 by p38 mitogen-activated protein kinases. Mol Cell Biol 22: 3892–3904.

- 601 20. Wang J, Yen A (2008) A MAPK-positive Feedback Mechanism for BLR1 Signaling  
602 Propels Retinoic Acid-triggered Differentiation and Cell Cycle Arrest. *J Biol Chem*  
603 283: 4375–4386.
- 604 21. Tasseff R, Nayak S, Song S, Yen A, Varner J (2011) Modeling and analysis of retinoic  
605 acid induced differentiation of uncommitted precursor cells. *Integr Biol* 3: 578 - 591.
- 606 22. Jensen HA, Styskal LE, Tasseff R, Bunaciu RP, Congleton J, et al. (2013) The  
607 src-family kinase inhibitor pp2 rescues inducible differentiation events in emergent  
608 retinoic acid-resistant myeloblastic leukemia cells. *PLoS One* 8: e58621.
- 609 23. Jensen HA, Bunaciu RP, Ibabao CN, Myers R, Varner JD, et al. (2014) Retinoic acid  
610 therapy resistance progresses from unilineage to bilineage in hl-60 leukemic blasts.  
611 *PLoS One* 9: e98929.
- 612 24. Jensen HA, Bunaciu RP, Varner JD, Yen A (2015) Gw5074 and pp2 kinase inhibitors  
613 implicate nontraditional c-raf and lyn function as drivers of retinoic acid-induced mat-  
614 uration. *Cell Signal* 27: 1666-75.
- 615 25. Jensen HA, Yourish HB, Bunaciu RP, Varner JD, Yen A (2015) Induced myelomono-  
616 cytic differentiation in leukemia cells is accompanied by noncanonical transcription  
617 factor expression. *FEBS Open Bio* 5: 789-800.
- 618 26. Milo R, Jorgensen P, Moran U, Weber G, Springer M (2010) Bionumbers—the  
619 database of key numbers in molecular and cell biology. *Nucleic Acids Res* 38: D750-  
620 3.
- 621 27. Katagiri K, Hattori S, Nakamura S, Yamamoto T, Yoshida T, et al. (1994) Activation  
622 of ras and formation of gap complex during tpa-induced monocytic differentiation of  
623 hl-60 cells. *Blood* 84: 1780–1789.
- 624 28. Miranda MB, Johnson DE (2007) Signal transduction pathways that contribute to  
625 myeloid differentiation. *Leukemia* 21: 1363–1377.
- 626 29. Hickstein DD, Back AL, Collins SJ (1989) Regulation of expression of the cd11b and

- 627 cd18 subunits of the neutrophil adherence receptor during human myeloid differen-  
628 tiation. *J Biol Chem* 264: 21812–21817.
- 629 30. Hornstein I, Alcover A, Katzav S (2004) Vav proteins, masters of the world of cy-  
630 toskeleton organization. *Cell Signal* 16: 1-11.
- 631 31. Song JS, Gomez J, Stancato LF, Rivera J (1996) Association of a p95 vav-containing  
632 signaling complex with the fcepsilonlonri gamma chain in the rbl-2h3 mast cell line.  
633 evidence for a constitutive in vivo association of vav with grb2, raf-1, and erk2 in an  
634 active complex. *J Biol Chem* 271: 26962–26970.
- 635 32. Costello PS, Walters AE, Mee PJ, Turner M, Reynolds LF, et al. (1999) The rho-  
636 family gtp exchange factor vav is a critical transducer of t cell receptor signals to the  
637 calcium, erk, and nf-kappab pathways. *Proc Natl Acad Sci U S A* 96: 3035–3040.
- 638 33. Graham D, Robertson C, Bautista J, Mascarenhas F, Diacovo M, et al. (2007)  
639 Neutrophil-mediated oxidative burst and host defense are controlled by a Vav-  
640 PLCgamma2 signaling axis in mice. *J Clin Invest* 117: 3445–3452.
- 641 34. Cleghon V, Morrison DK (1994) Raf-1 interacts with fyn and src in a non-  
642 phosphotyrosine-dependent manner. *J Biol Chem* 269: 17749–17755.
- 643 35. Zimmermann S, Moelling K (1999) Phosphorylation and regulation of raf by akt (pro-  
644 tein kinase b). *Science* 286: 1741–1744.
- 645 36. Ritt DA, Zhou M, Conrads TP, Veenstra TD, Copeland TD, et al. (2007) Ck2 is a  
646 component of the ksr1 scaffold complex that contributes to raf kinase activation.  
647 *Curr Biol* 17: 179–184.
- 648 37. Hekman M, Wiese S, Metz R, Albert S, Troppmair J, et al. (2004) Dynamic changes  
649 in c-raf phosphorylation and 14-3-3 protein binding in response to growth factor stim-  
650 ulation: differential roles of 14-3-3 protein binding sites. *J Biol Chem* 279: 14074–  
651 14086.
- 652 38. Dhillon AS, Yip YY, Grindlay GJ, Pakay JL, Dangers M, et al. (2009) The c-terminus

- 653 of raf-1 acts as a 14-3-3-dependent activation switch. *Cell Signal* 21: 1645–1651.
- 654 39. Kim HS, Lim IK (2009) Phosphorylated extracellular signal-regulated protein kinases  
655 1 and 2 phosphorylate sp1 on serine 59 and regulate cellular senescence via tran-  
656 scription of p21sdi1/cip1/waf1. *J Biol Chem* 284: 15475–15486.
- 657 40. Milanini-Mongiat J, Pouyss?gur J, Pag? G (2002) Identification of two sp1 phos-  
658 phorylation sites for p42/p44 mitogen-activated protein kinases: their implication in  
659 vascular endothelial growth factor gene transcription. *J Biol Chem* 277: 20631–  
660 20639.
- 661 41. Zhang Y, Cho YY, Petersen BL, Zhu F, Dong Z (2004) Evidence of stat1 phosphory-  
662 lation modulated by mapks, mek1 and msk1. *Carcinogenesis* 25: 1165–1175.
- 663 42. Li Z, Theus MH, Wei L (2006) Role of erk 1/2 signaling in neuronal differentiation of  
664 cultured embryonic stem cells. *Dev Growth Differ* 48: 513–523.
- 665 43. Yen A, Reece SL, Albright KL (1984) Dependence of hl-60 myeloid cell differentiation  
666 on continuous and split retinoic acid exposures: precommitment memory associated  
667 with altered nuclear structure. *J Cell Physiol* 118: 277–286.
- 668 44. Ferrell J (2002) Self-perpetuating states in signal transduction: positive feedback,  
669 double-negative feedback and bistability. *Curr Opin Cell Biol* 14: 140-8.
- 670 45. Xiong W, Ferrell J (2003) A positive-feedback-based bistable 'memory module' that  
671 governs a cell fate decision. *Nature* 426: 460-5.
- 672 46. Bagci EZ, Vodovotz Y, Billiar TR, Ermentrout GB, Bahar I (2006) Bistability in apop-  
673 tosis: roles of bax, bcl-2, and mitochondrial permeability transition pores. *Biophys J*  
674 90: 1546-59.
- 675 47. Luan D, Zai M, Varner JD (2007) Computationally derived points of fragility of a  
676 human cascade are consistent with current therapeutic strategies. *PLoS Comput  
677 Biol* 3: e142.
- 678 48. Moon TS, Lou C, Tamsir A, Stanton BC, Voigt CA (2012) Genetic programs con-

- 679       structured from layered logic gates in single cells. *Nature* 491: 249-53.
- 680   49. Wayman JA, Sagar A, Varner JD (2015) Dynamic modeling of cell-free biochemical  
681       networks using effective kinetic models. *Processes* 3: 138.
- 682   50. Igel C, Hansen N, Roth S (2007) Covariance matrix adaptation for multi-objective  
683       optimization. *Evol Comput* 15: 1-28.
- 684   51. Bezanson J, Edelman A, Karpinski S, Shah VB (2014) Julia: A fresh approach to  
685       numerical computing. *CoRR* abs/1411.1607.
- 686   52. Brooks SC, Kazmer S, Levin AA, Yen A (1996) Myeloid differentiation and retinoblas-  
687       toma phosphorylation changes in HL-60 cells induced by retinoic acid receptor- and  
688       retinoid X receptor-selective retinoic acid analogs. *Blood* 87: 227-237.
- 689   53. Rishi AK, Gerald TM, Shao ZM, Li XS, Baumann RG, et al. (1996) Regulation of the  
690       human retinoic acid receptor alpha gene in the estrogen receptor negative human  
691       breast carcinoma cell lines skbr-3 and mda-mb-435. *Cancer Res* 56: 5246-52.
- 692   54. Mueller BU, Pabst T, Fos J, Petkovic V, Fey MF, et al. (2006) Atra resolves the dif-  
693       ferentiation block in t(15;17) acute myeloid leukemia by restoring pu.1 expression.  
694       Blood 107: 3330-8.
- 695   55. Friedman AD (2007) Transcriptional control of granulocyte and monocyte develop-  
696       ment. *Oncogene* 26: 6816-28.
- 697   56. Luo XM, Ross AC (2006) Retinoic acid exerts dual regulatory actions on the ex-  
698       pression and nuclear localization of interferon regulatory factor-1. *Exp Biol Med*  
699       (Maywood) 231: 619-31.
- 700   57. Sylvester I, Schöler HR (1994) Regulation of the oct-4 gene by nuclear receptors.  
701       *Nucleic Acids Res* 22: 901-11.
- 702   58. Drach J, McQueen T, Engel H, Andreeff M, Robertson KA, et al. (1994) Retinoic  
703       acid-induced expression of cd38 antigen in myeloid cells is mediated through  
704       retinoic acid receptor-alpha. *Cancer Res* 54: 1746-52.

- 705 59. Liu M, Iavarone A, Freedman LP (1996) Transcriptional activation of the human  
706 p21(waf1/cip1) gene by retinoic acid receptor. correlation with retinoid induction of  
707 u937 cell differentiation. J Biol Chem 271: 31723-8.
- 708 60. Bunaciu RP, Yen A (2013) 6-formylindolo (3,2-b)carbazole (ficz) enhances retinoic  
709 acid (ra)-induced differentiation of hl-60 myeloblastic leukemia cells. Mol Cancer 12:  
710 39.
- 711 61. Balmer JE, Blomhoff R (2002) Gene expression regulation by retinoic acid. J Lipid  
712 Res 43: 1773-808.
- 713 62. Rosen ED, Hsu CH, Wang X, Sakai S, Freeman MW, et al. (2002) C/ebpalpha in-  
714 duces adipogenesis through ppargamma: a unified pathway. Genes Dev 16: 22-6.
- 715 63. Varley CL, Bacon EJ, Holder JC, Southgate J (2009) Foxa1 and irf-1 intermediary  
716 transcriptional regulators of ppargamma-induced urothelial cytodifferentiation. Cell  
717 Death Differ 16: 103-14.
- 718 64. Bruemmer D, Yin F, Liu J, Berger JP, Sakai T, et al. (2003) Regulation of the growth  
719 arrest and dna damage-inducible gene 45 (gadd45) by peroxisome proliferator-  
720 activated receptor gamma in vascular smooth muscle cells. Circ Res 93: e38-47.
- 721 65. Delerive P, De Bosscher K, Besnard S, Vanden Berghe W, Peters JM, et al. (1999)  
722 Peroxisome proliferator-activated receptor alpha negatively regulates the vascular  
723 inflammatory gene response by negative cross-talk with transcription factors nf-  
724 kappaB and ap-1. J Biol Chem 274: 32048-54.
- 725 66. Altinok S, Xu M, Spiegelman BM (1997) Ppargamma induces cell cycle withdrawal:  
726 inhibition of e2f/dp dna-binding activity via down-regulation of pp2a. Genes Dev 11:  
727 1987-98.
- 728 67. Fei J, Cook C, Gillespie M, Yu B, Fullen K, et al. (2011) Atherogenic  $\omega$ -6 lipids mod-  
729 ulate ppar- egr-1 crosstalk in vascular cells. PPAR Res 2011: 753917.
- 730 68. Song EK, Lee YR, Kim YR, Yeom JH, Yoo CH, et al. (2012) Naadp mediates insulin-

- 731 stimulated glucose uptake and insulin sensitization by ppar $\gamma$  in adipocytes. Cell Rep  
732 2: 1607-19.
- 733 69. Szanto A, Nagy L (2005) Retinoids potentiate peroxisome proliferator-activated re-  
734 ceptor gamma action in differentiation, gene expression, and lipid metabolic pro-  
735 cesses in developing myeloid cells. Mol Pharmacol 67: 1935-43.
- 736 70. Han S, Sidell N, Fisher PB, Roman J (2004) Up-regulation of p21 gene expres-  
737 sion by peroxisome proliferator-activated receptor gamma in human lung carcinoma  
738 cells. Clin Cancer Res 10: 1911-9.
- 739 71. Von Knethen A, Brüne B (2002) Activation of peroxisome proliferator-activated re-  
740 ceptor gamma by nitric oxide in monocytes/macrophages down-regulates p47phox  
741 and attenuates the respiratory burst. J Immunol 169: 2619-26.
- 742 72. Dispirito JR, Fang B, Wang F, Lazar MA (2013) Pruning of the adipocyte peroxisome  
743 proliferator-activated receptor  $\gamma$  cistrome by hematopoietic master regulator pu.1.  
744 Mol Cell Biol 33: 3354-64.
- 745 73. Chen H, Ray-Gallet D, Zhang P, Hetherington CJ, Gonzalez DA, et al. (1995) Pu.1  
746 (spi-1) autoregulates its expression in myeloid cells. Oncogene 11: 1549-60.
- 747 74. Steidl U, Rosenbauer F, Verhaak RGW, Gu X, Ebralidze A, et al. (2006) Essential  
748 role of jun family transcription factors in pu.1 knockdown-induced leukemic stem  
749 cells. Nat Genet 38: 1269-77.
- 750 75. Laslo P, Spooner CJ, Warmflash A, Lancki DW, Lee HJ, et al. (2006) Multilineage  
751 transcriptional priming and determination of alternate hematopoietic cell fates. Cell  
752 126: 755-66.
- 753 76. Pahl HL, Scheibe RJ, Zhang DE, Chen HM, Galson DL, et al. (1993) The proto-  
754 oncogene pu.1 regulates expression of the myeloid-specific cd11b promoter. J Biol  
755 Chem 268: 5014-20.
- 756 77. Yuki H, Ueno S, Tatetsu H, Niiro H, Iino T, et al. (2013) Pu.1 is a potent tumor

- 757 suppressor in classical hodgkin lymphoma cells. Blood 121: 962-70.
- 758 78. Li SL, Schlegel W, Valente AJ, Clark RA (1999) Critical flanking sequences of pu.1  
759 binding sites in myeloid-specific promoters. J Biol Chem 274: 32453-60.
- 760 79. Dahl R, Walsh JC, Lancki D, Laslo P, Iyer SR, et al. (2003) Regulation of macrophage  
761 and neutrophil cell fates by the pu.1:c/ebpalpha ratio and granulocyte colony-  
762 stimulating factor. Nat Immunol 4: 1029-36.
- 763 80. Timchenko N, Wilson DR, Taylor LR, Abdelsayed S, Wilde M, et al. (1995) Autoreg-  
764 ulation of the human c/ebp alpha gene by stimulation of upstream stimulatory factor  
765 binding. Mol Cell Biol 15: 1192-202.
- 766 81. Lidonnici MR, Audia A, Soliera AR, Prisco M, Ferrari-Amorotti G, et al. (2010) Ex-  
767 pression of the transcriptional repressor gfi-1 is regulated by c/ebpalpha and is  
768 involved in its proliferation and colony formation-inhibitory effects in p210bcr/abl-  
769 expressing cells. Cancer Res 70: 7949-59.
- 770 82. D'Alo' F, Johansen LM, Nelson EA, Radomska HS, Evans EK, et al. (2003) The  
771 amino terminal and e2f interaction domains are critical for c/ebp alpha-mediated  
772 induction of granulopoietic development of hematopoietic cells. Blood 102: 3163-  
773 71.
- 774 83. Pan Z, Hetherington CJ, Zhang DE (1999) Ccaat/enhancer-binding protein activates  
775 the cd14 promoter and mediates transforming growth factor beta signaling in mono-  
776 cyte development. J Biol Chem 274: 23242-8.
- 777 84. Harris TE, Albrecht JH, Nakanishi M, Darlington GJ (2001) Ccaat/enhancer-binding  
778 protein-alpha cooperates with p21 to inhibit cyclin-dependent kinase-2 activity and  
779 induces growth arrest independent of dna binding. J Biol Chem 276: 29200-9.
- 780 85. Bauvois B, Durant L, Laboureau J, Barthélémy E, Rouillard D, et al. (1999) Upreg-  
781 ulation of cd38 gene expression in leukemic b cells by interferon types i and ii. J  
782 Interferon Cytokine Res 19: 1059-66.

- 783 86. Passioura T, Dolnikov A, Shen S, Symonds G (2005) N-ras-induced growth suppres-  
784 sion of myeloid cells is mediated by irf-1. *Cancer Res* 65: 797-804.
- 785 87. Dahl R, Iyer SR, Owens KS, Cuylear DD, Simon MC (2007) The transcriptional  
786 repressor gfi-1 antagonizes pu.1 activity through protein-protein interaction. *J Biol  
787 Chem* 282: 6473-83.
- 788 88. Duan Z, Horwitz M (2003) Targets of the transcriptional repressor oncoprotein gfi-1.  
789 *Proc Natl Acad Sci U S A* 100: 5932-7.
- 790 89. Chen H, Zhang P, Radomska HS, Hetherington CJ, Zhang DE, et al. (1996) Octamer  
791 binding factors and their coactivator can activate the murine pu.1 (spi-1) promoter.  
792 *J Biol Chem* 271: 15743-52.
- 793 90. Behre G, Whitmarsh AJ, Coghlan MP, Hoang T, Carpenter CL, et al. (1999) c-jun  
794 is a jnk-independent coactivator of the pu.1 transcription factor. *J Biol Chem* 274:  
795 4939-46.
- 796 91. Kardassis D, Papakosta P, Pardali K, Moustakas A (1999) c-jun transactivates the  
797 promoter of the human p21(waf1/cip1) gene by acting as a superactivator of the  
798 ubiquitous transcription factor sp1. *J Biol Chem* 274: 29572-81.
- 799 92. Johnson DG, Ohtani K, Nevins JR (1994) Autoregulatory control of e2f1 expression  
800 in response to positive and negative regulators of cell cycle progression. *Genes Dev*  
801 8: 1514-25.
- 802 93. Fu M, Zhang J, Lin Y, Zhu X, Ehrengruber MU, et al. (2002) Early growth response  
803 factor-1 is a critical transcriptional mediator of peroxisome proliferator-activated  
804 receptor-gamma 1 gene expression in human aortic smooth muscle cells. *J Biol  
805 Chem* 277: 26808-14.
- 806 94. Mak KS, Funnell APW, Pearson RCM, Crossley M (2011) Pu.1 and haematopoietic  
807 cell fate: Dosage matters. *Int J Cell Biol* 2011: 808524.
- 808 95. Chen F, Wang Q, Wang X, Studzinski GP (2004) Up-regulation of egr1 by 1,25-

- 809 dihydroxyvitamin d3 contributes to increased expression of p35 activator of cyclin-  
810 dependent kinase 5 and consequent onset of the terminal phase of hl60 cell differ-  
811 entiation. *Cancer Res* 64: 5425-33.
- 812 96. Suh J, Jeon YJ, Kim HM, Kang JS, Kaminski NE, et al. (2002) Aryl hydrocarbon  
813 receptor-dependent inhibition of ap-1 activity by 2,3,7,8-tetrachlorodibenzo-p-dioxin  
814 in activated b cells. *Toxicol Appl Pharmacol* 181: 116-23.
- 815 97. Shen M, Bunaciu RP, Congleton J, Jensen HA, Sayam LG, et al. (2011) Inter-  
816 feron regulatory factor-1 binds c-cbl, enhances mitogen activated protein kinase  
817 signaling and promotes retinoic acid-induced differentiation of hl-60 human myelo-  
818 monoblastic leukemia cells. *Leuk Lymphoma* 52: 2372-9.
- 819 98. Bunaciu RP, Yen A (2011) Activation of the aryl hydrocarbon receptor ahr promotes  
820 retinoic acid-induced differentiation of myeloblastic leukemia cells by restricting ex-  
821 pression of the stem cell transcription factor oct4. *Cancer Res* 71: 2371-80.
- 822 99. Jackson DA, Pombo A, Iborra F (2000) The balance sheet for transcription: an anal-  
823 ysis of nuclear rna metabolism in mammalian cells. *FASEB J* 14: 242-54.
- 824 100. Zhao ZW, Roy R, Gebhardt JCM, Suter DM, Chapman AR, et al. (2014) Spatial orga-  
825 nization of rna polymerase ii inside a mammalian cell nucleus revealed by reflected  
826 light-sheet superresolution microscopy. *Proc Natl Acad Sci U S A* 111: 681-6.
- 827 101. Freitas R, Merkle R (2004) Kinematic Self-Replicating Machines. Oxford University  
828 Press.
- 829 102. Yang E, van Nimwegen E, Zavolan M, Rajewsky N, Schroeder M, et al. (2003) De-  
830 cay rates of human mrnas: correlation with functional characteristics and sequence  
831 attributes. *Genome Res* 13: 1863-72.
- 832 103. Doherty MK, Hammond DE, Clague MJ, Gaskell SJ, Beynon RJ (2009) Turnover  
833 of the human proteome: determination of protein intracellular stability by dynamic  
834 silac. *J Proteome Res* 8: 104-12.

- 835 104. Darzacq X, Shav-Tal Y, de Turris V, Brody Y, Shenoy SM, et al. (2007) In vivo dy-  
836 namics of rna polymerase ii transcription. Nat Struct Mol Biol 14: 796-806.
- 837 105. Boström K, Wettsten M, Borén J, Bondjers G, Wiklund O, et al. (1986) Pulse-chase  
838 studies of the synthesis and intracellular transport of apolipoprotein b-100 in hep g2  
839 cells. J Biol Chem 261: 13800-6.
- 840 106. Meyers R, editor (2004) Encyclopedia of Molecular Cell Biology and Molecular  
841 Medicine, Volume 1, 2nd Edition. ISBN: 978-3-527-30543-8. Wiley-Blackwell.
- 842 107. Rosenbluth MJ, Lam WA, Fletcher DA (2006) Force microscopy of nonadherent  
843 cells: a comparison of leukemia cell deformability. Biophys J 90: 2994-3003.

**Table 1:** Myelomonocytic transcription factor connectivity used in the signal integration and phenotype modules.

844

845

Effector	Effect	Target	Source
RAR $\alpha$	+	RAR $\alpha$	(53)
	+	PU.1	(54)
	+	C/EBP $\alpha$	(55)
	+	IRF-1	(56)
	-	Oct4	(57)
	+	CD38	(58)
	+	p21	(59)
	+	AhR	(60)
	+	EGR1	(61)
PPAR $\gamma$	+	C/EBP $\alpha$	(62)
	+	IRF-1	(63)
	+	Oct1	(64)
	-	AP-1	(65)
	-	E2F	(66)
	-	EGR1	(67)
	+	CD38	(68)
	+	CD14	(69)
	+	p21	(70)
	-	p47phox	(71)
PU.1	-	PPAR $\gamma$	(72)
	+	PU.1	(73)
	+	AP-1	(74)
	+	EGR1	(75)
	+	CD11b	(76)
	+	p21	(77)
	+	p47phox	(78)
C/EBP $\alpha$	+	PPAR $\gamma$	(62)
	+	PU.1	(79)
	+	C/EBP $\alpha$	(80)
	+	Gfi-1	(81)
	-	E2F	(82)
	+	CD14	(83)

	+	p21	(84)
IRF-1	+	CD38	(85)
	+	p21	(86)
	-	PU.1	(87)
	-	C/EBP $\alpha$	(88)
	-	E2F	(88)
	-	EGR1	(75)
	-	p21	(88)
Oct1	+	PU.1	(89)
AP-1	-	PPAR $\gamma$	(65)
	+	PU.1	(90)
	+	p21	(91)
E2F	+	E2F	(92)
EGR1	+	PPAR $\gamma$	(93)
	-	Gfi-1	(94)
	+	CD14	(95)
AhR	+	AP-1	(96)
	+	IRF-1	(97)
	-	Oct4	(98)
	-	PU.1	

**Table 2:** Characteristic model parameters estimated from literature.

Symbol	Description	Value	Units	Source	
$R_1$	RNA polymerase abundance	75,000	copies/cell	(99, 100)	
$R_2$	Ribosome abundance	$1 \times 10^6$	copies/cell	(101)	
$G_i$	Characteristic gene abundance	2	copies/cell	this study	
$K_X$	Saturation constant transcription	4,600	copies/cell	this study	
$K_T$	Saturation constant translation	100,000	copies/cell	this study	
$t_{1/2,m}$	characteristic mRNA half-life (transcription factor)	2	hr	(102)	
$t_{1/2,p}$	characteristic protein half-life	10	hr	(103)	
$\theta_{m,j}$	characteristic mRNA degradation constant	0.34	$hr^{-1}$	derived	
$\theta_{p,j}$	characteristic protein degradation constant	0.07	$hr^{-1}$	derived	
848	$t_d$	HL-60 doubling time	19.5	hr	this study
	$\mu$	growth rate	0.035	$hr^{-1}$	derived
	$k_d$	death rate	$0.10\mu$	$hr^{-1}$	derived
$e_T$	elongation rate RNA polymerase	6	nt/s	(104)	
$e_X$	elongation rate Ribosome	5	aa/s	(105)	
$L_{T,o}$	characteristic gene length	15,000	nt	(106)	
$L_{X,o}$	characteristic transcript length	5,000	nt	derived	
$k_T$	characteristic transcription rate	1.44	$hr^{-1}$	derived	
$k_X$	characteristic translation rate	3.60	$hr^{-1}$	derived	
$D$	Diameter of an HL-60 cell	12.4	$\mu m^3$	(107)	
$f_C$	cytoplasmic fraction	0.51	dimensionless	(107)	

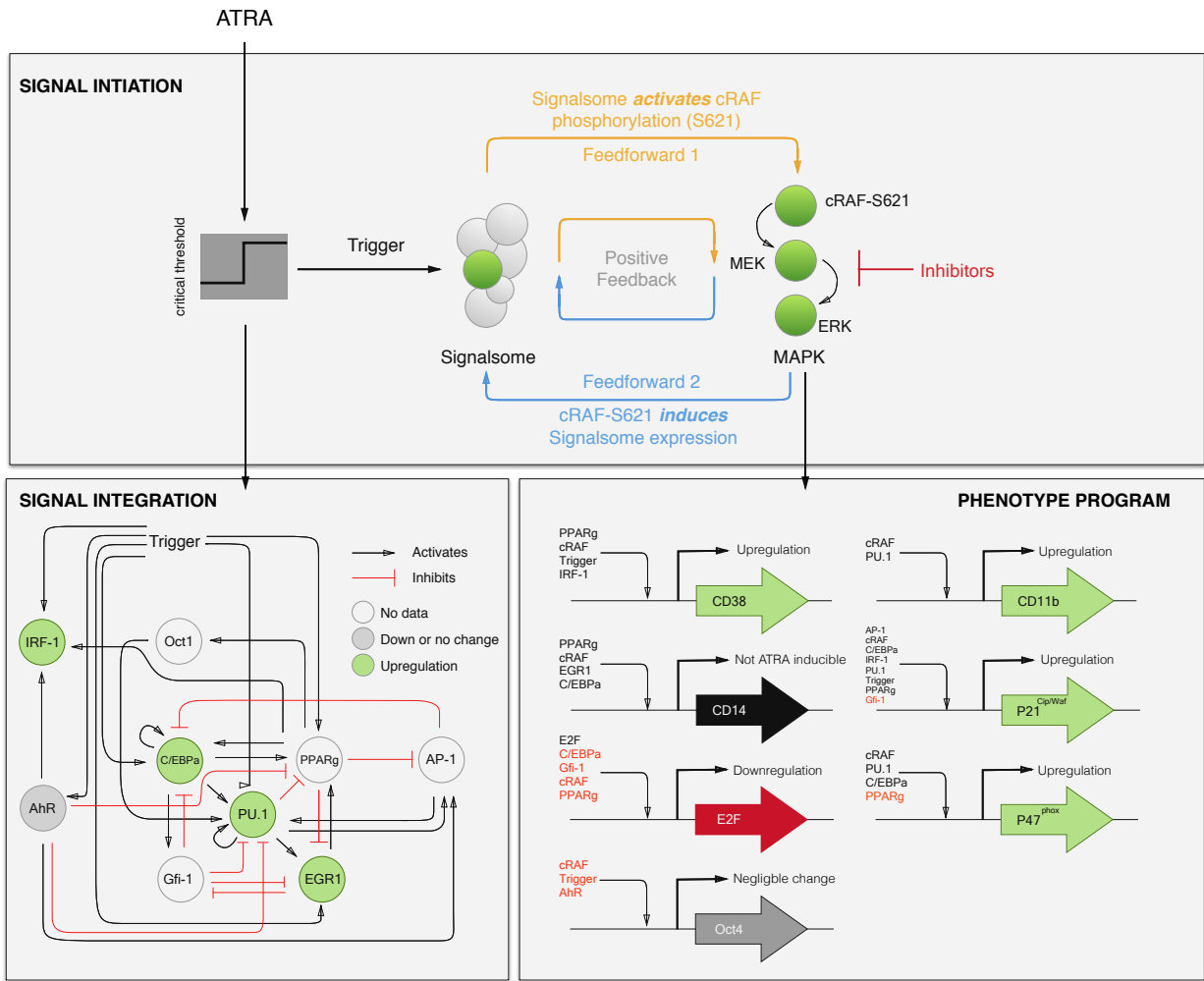


**Fig. 1:** Schematic of the effective ATRA differentiation circuit. Above a critical threshold, ATRA activates an upstream Trigger, which induces signalsome complex formation. Signalsome activates the mitogen-activated protein kinase (MAPK) cascade which in turn drives the differentiation program and signalsome formation. Both Trigger and activated cRaf-pS621 drive a phenotype gene expression program responsible for differentiation. Trigger activates the expression of a series of transcription factors which in combination with cRaf-pS621 result in phenotypic change.

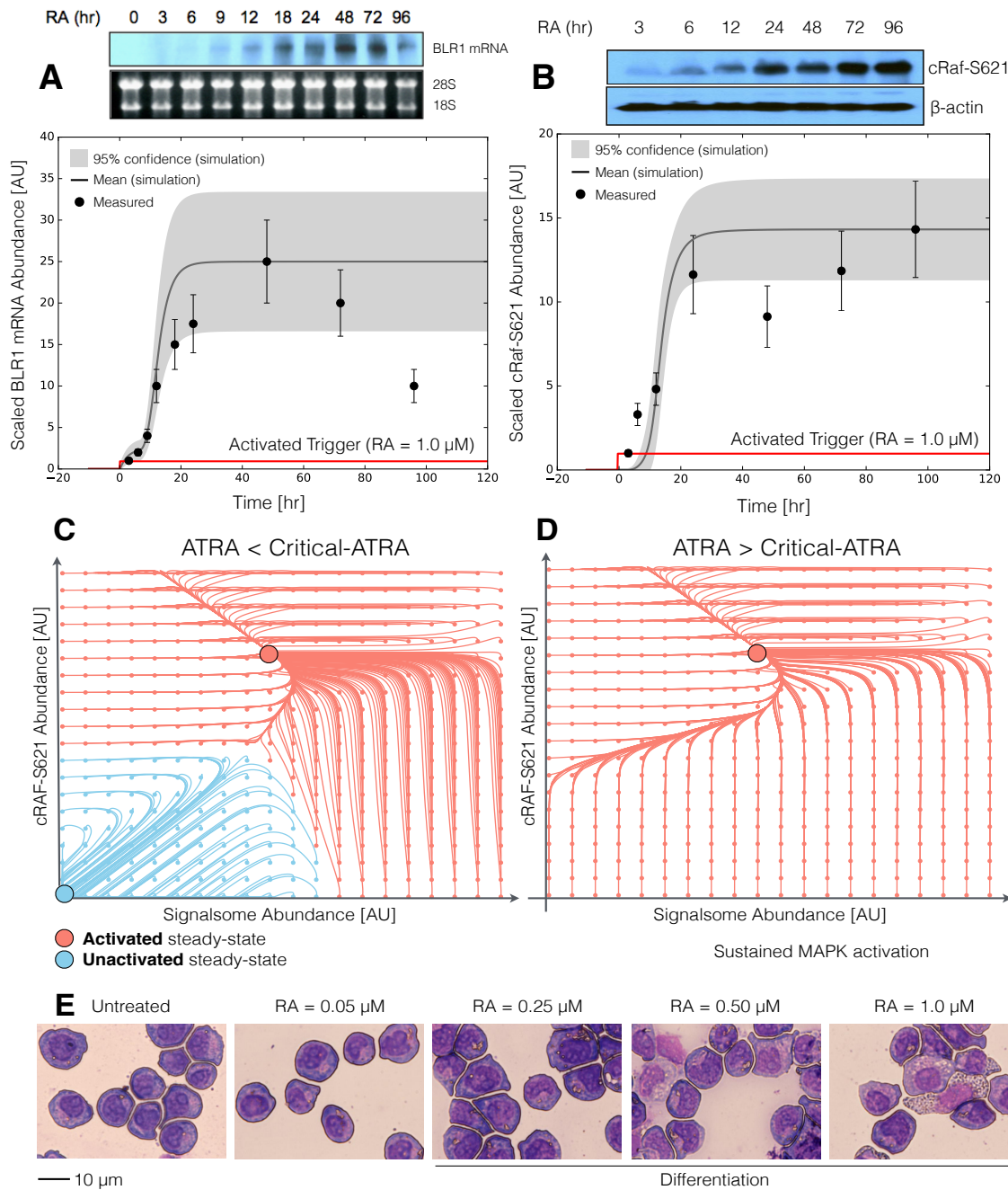


**Fig. 2:** Model analysis for ATRA-induced HL-60 differentiation. A: BLR1 mRNA versus time following exposure to  $1\mu\text{M}$  ATRA at  $t = 0$  hr. B: cRaf-pS621 versus time following exposure to  $1\mu\text{M}$  ATRA at  $t = 0$  hr. Points denote experimental measurements, solid lines denote the mean model performance. Shaded regions denote the 99% confidence interval calculated over the parameter ensemble. C: Signalsome and cRaf-pS621 nullclines for ATRA below the critical threshold. The model had two stable steady states and a single unstable state in this regime. D: Signalsome and cRaf-pS621 nullclines for ATRA above the critical threshold. In this regime the model had only a single stable steady state. E: Morphology of HL-60 as a function of ATRA concentration ( $t = 72$  hr).

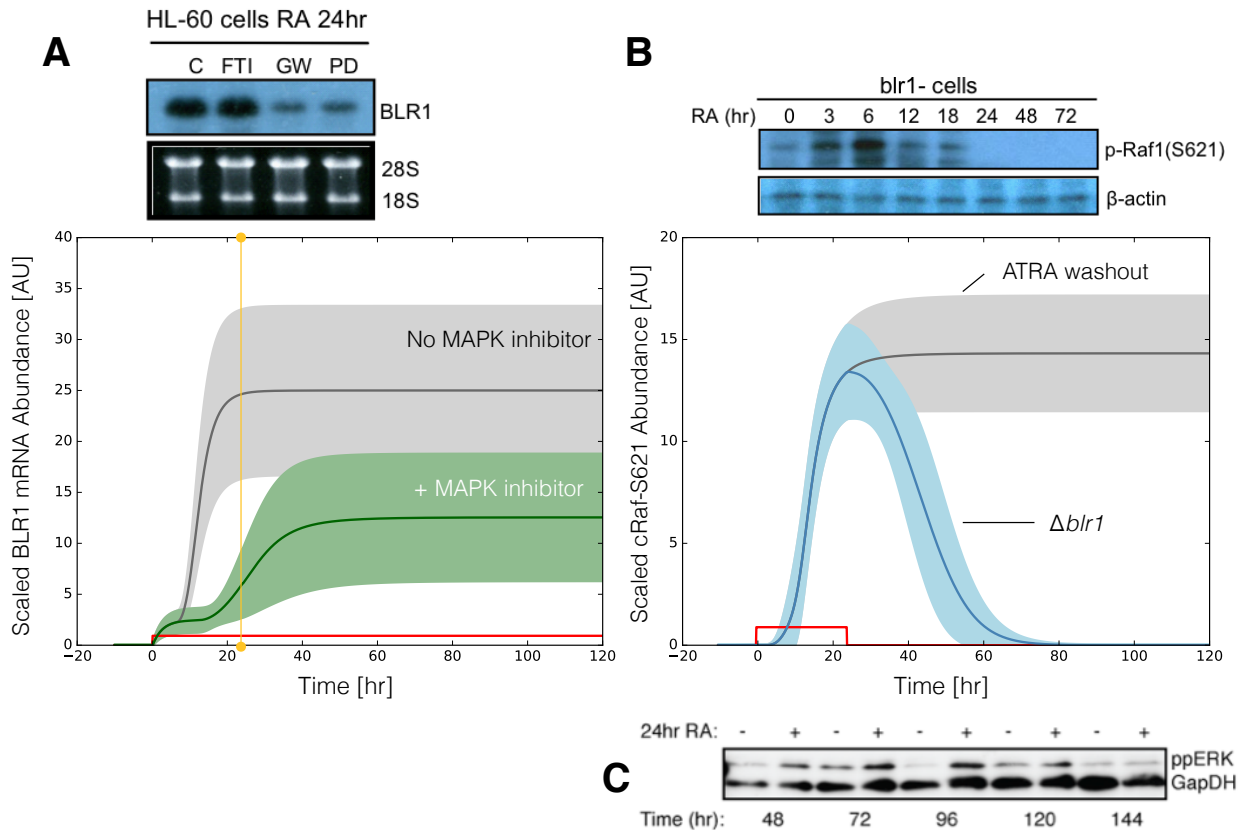


**Fig. 3:** Model simulation following exposure to  $1\mu\text{M}$  ATRA. A: BLR1 mRNA versus time with and without MAPK inhibitor. B: cRaf-pS621 versus time following pulsed exposure to  $1\mu\text{M}$  ATRA with and without BLR1. Solid lines denote the mean model performance, while shaded regions denote the 99% confidence interval calculated over the parameter ensemble. C: Western blot analysis of phosphorylated ERK1/2 in ATRA washout experiments. Experimental data in panels A and B were reproduced from Wang and Yen (20), data in panel C is reported in this study.

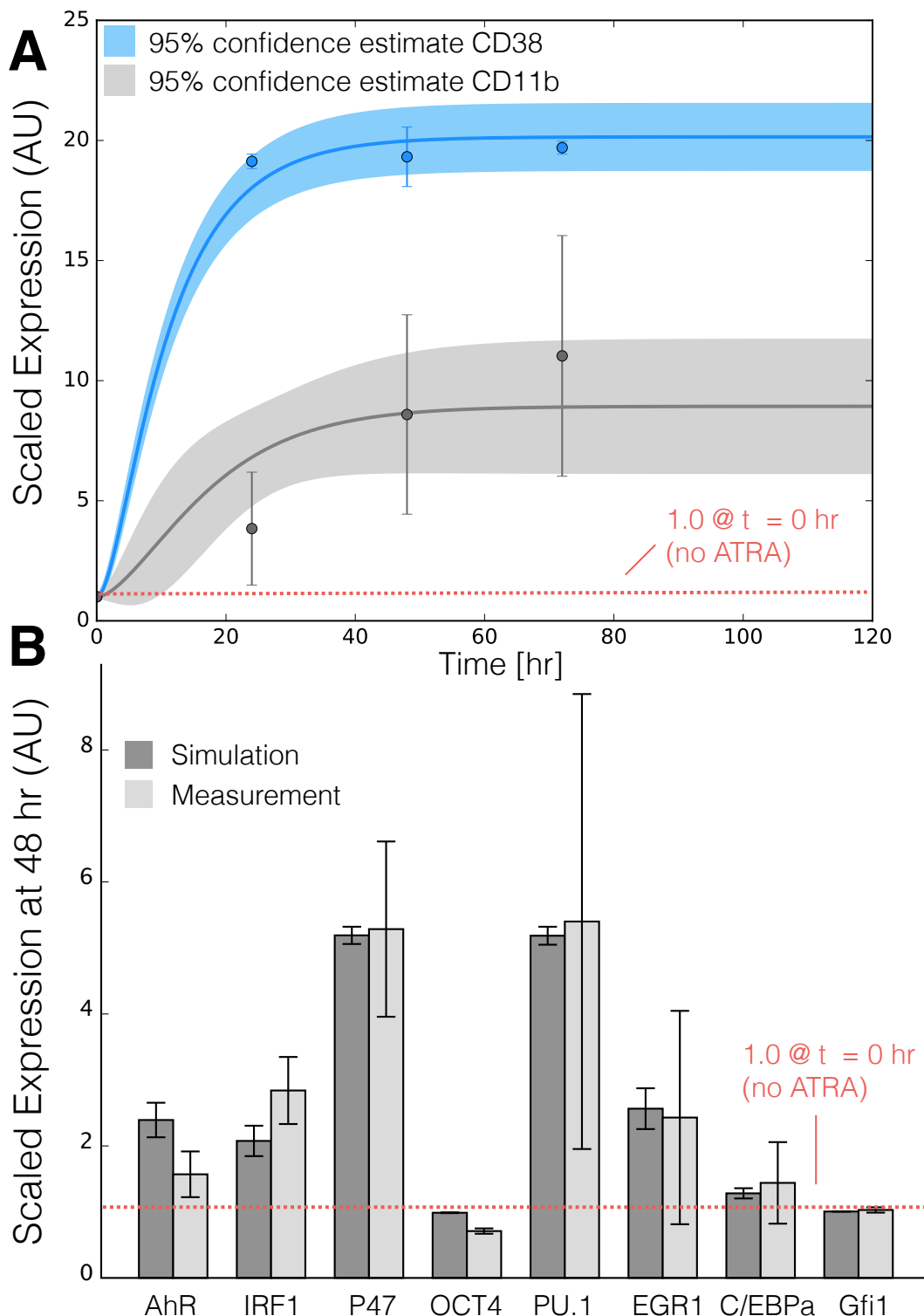


**Fig. 4:** Model simulation of the HL-60 gene expression program following exposure to  $1\mu\text{M}$  ATRA at  $t = 0$  hr. A: CD38 and CD11b expression versus time following ATRA exposure at time  $t = 0$  hr. B: Gene expression at  $t = 48$  hr following ATRA exposure. Experimental data in panels A and B were reproduced from Jensen et al. (25).

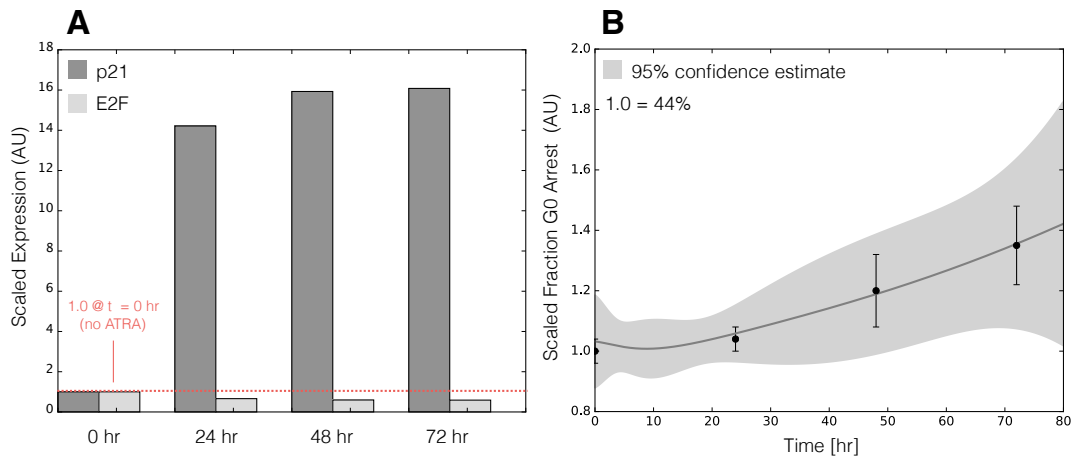


**Fig. 5:** Model simulation of HL-60 cell-cycle arrest following exposure to  $1\mu\text{M}$  ATRA at  $t = 0$  hr. A: Predicted p21 and E2F expression levels for the best parameter set following ATRA exposure at time  $t = 0$  hr. B: Estimated fraction of HL-60 cells in G0 arrest following ATRA exposure at time  $t = 0$  hr. The gray region denotes the 95% confidence estimate of the polynomial model. Experimental data in panel B was reproduced from Jensen et al. (25).

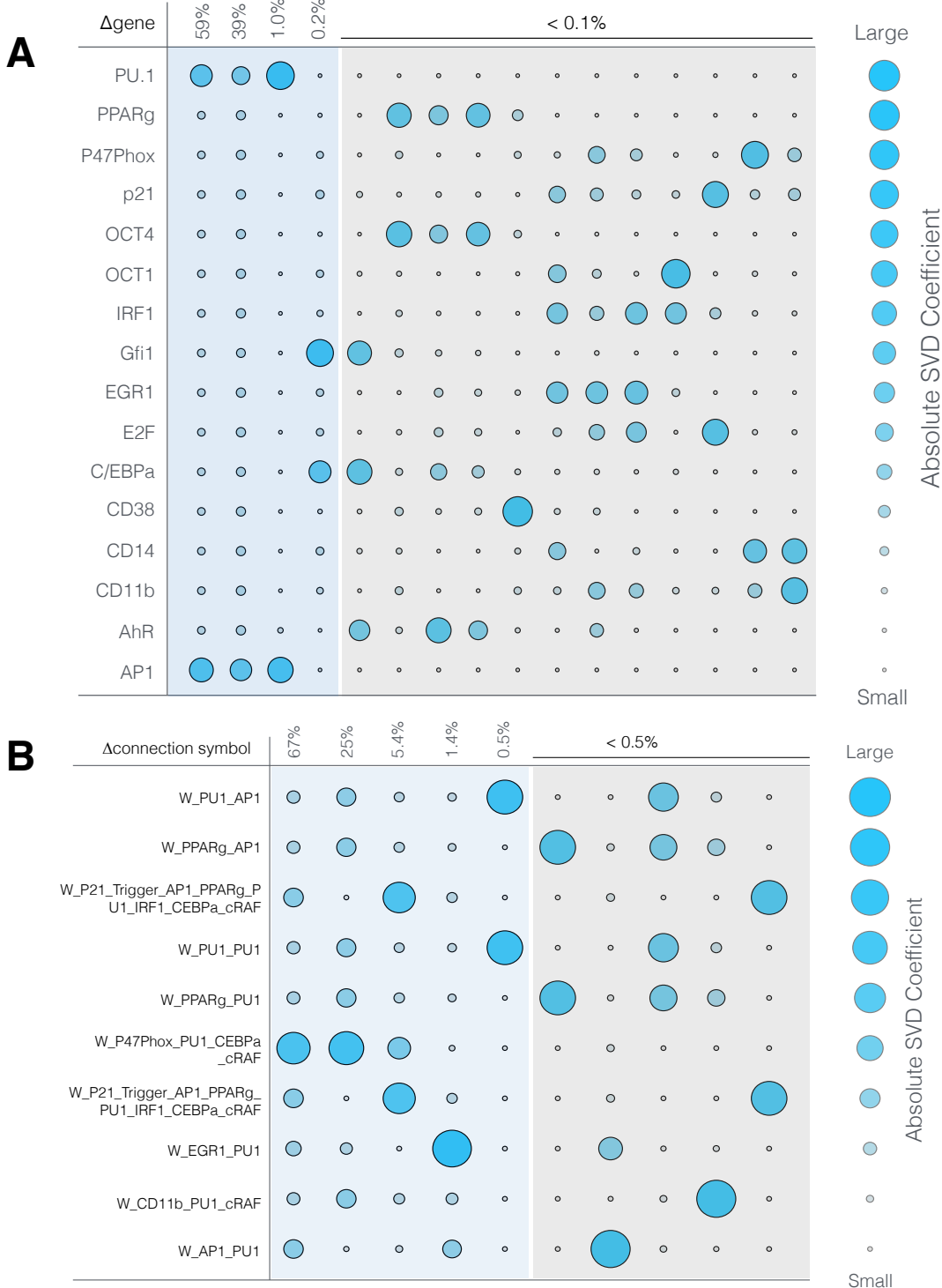


**Fig. 6:** Robustness of the HL-60 differentiation program following exposure to  $1\mu\text{M}$  ATRA at  $t = 0$  hr. A: Singular value decomposition of the system response ( $l^2$ -norm between the perturbed and nominal state) following pairwise gene knockout simulations using the best fit parameter set. The percentage at the top of each column describes the fraction of the variance in the system state captured by the node combinations in the rows. B: Singular value decomposition of the system response ( $l^2$ -norm between the perturbed and nominal state) following the pairwise removal of connections from the PU.1 and AP1 nodes.

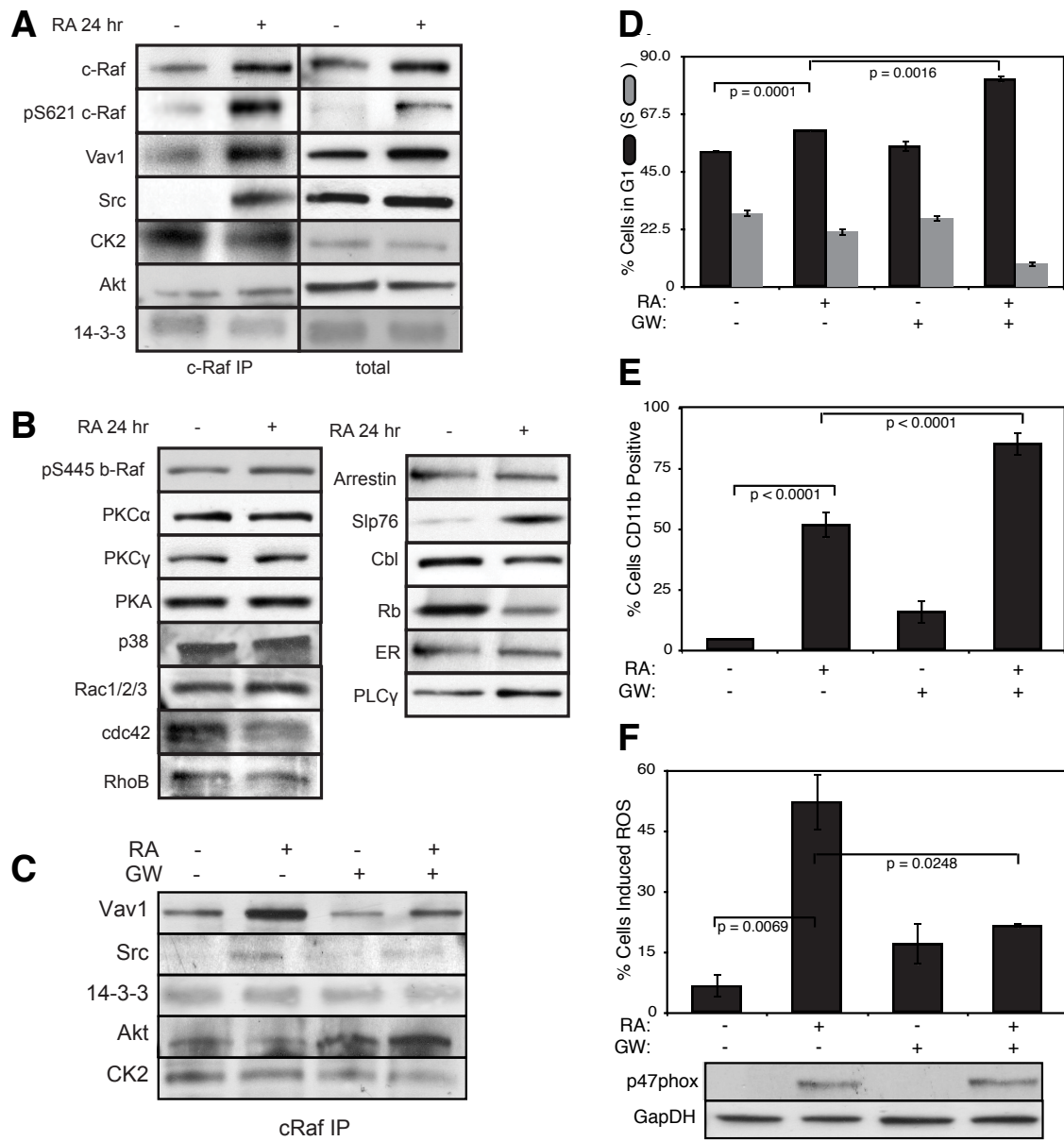


**Fig. 7:** Investigation of a panel of possible Raf interaction partners in the presence and absence of ATRA. A: Species identified to precipitate out with Raf: first column shows Western blot analysis on total Raf immunoprecipitation with and without 24 hr ATRA treatment and the second on total lysate. B: The expression of species considered that did not precipitate out with Raf at levels detectable by Western blot analysis on total lysate. C: Effect of the Raf inhibitor GW5074 on Raf interactions as determined by Western blot analysis of total Raf immunoprecipitation. The Authors note the signal associated with Src was found to be weak. D: Cell Cycle distribution as determined by flow cytometry indicated arrest induced by ATRA, which was increased by the addition of GW5074. E: Expression of the cell surface marker CD11b as determined by flow cytometry indicated increased expression induced by ATRA, which was enhanced by the addition of GW5074. F: Inducible reactive oxygen species (ROS) as determined by DCF flow cytometry. The functional differentiation response of ATRA treated cells was mitigated by GW5074.